NASA / CR-2000-210297

Electromagnetic Field Penetration Studies

M. D. Deshpande
NYMA, Inc., Hampton, Virginia

June 2000

The NASA STI Program Office . . . in Profile

Since its founding, NASA has been dedicated to the advancement of aeronautics and space science. The NASA Scientific and Technical Information (STI) Program Office plays a key part in helping NASA maintain this important role.

The NASA STI Program Office is operated by Langley Research Center, the lead center for NASA's scientific and technical information. The NASA STI Program Office provides access to the NASA STI Database, the largest collection of aeronautical and space science STI in the world. The Program Office is also NASA's institutional mechanism for disseminating the results of its research and development activities. These results are published by NASA in the NASA STI Report Series, which includes the following report types:

- TECHNICAL PUBLICATION. Reports of completed research or a major significant phase of research that present the results of NASA programs and include extensive data or theoretical analysis. Includes compilations of significant scientific and technical data and information deemed to be of continuing reference value. NASA counterpart of peer-reviewed formal professional papers, but having less stringent limitations on manuscript length and extent of graphic presentations.

- TECHNICAL MEMORANDUM. Scientific and technical findings that are preliminary or of specialized interest, e.g., quick release reports, working papers, and bibliographies that contain minimal annotation. Does not contain extensive analysis.

- CONTRACTOR REPORT. Scientific and technical findings by NASA-sponsored contractors and grantees.

- CONFERENCE PUBLICATION. Collected papers from scientific and technical conferences, symposia, seminars, or other meetings sponsored or co-sponsored by NASA.

- SPECIAL PUBLICATION. Scientific, technical, or historical information from NASA programs, projects, and missions, often concerned with subjects having substantial public interest.

- TECHNICAL TRANSLATION. English-language translations of foreign scientific and technical material pertinent to NASA's mission.

Specialized services that complement the STI Program Office's diverse offerings include creating custom thesauri, building customized databases, organizing and publishing research results . . . even providing videos.

For more information about the NASA STI Program Office, see the following:

- Access the NASA STI Program Home Page at *http://www.sti.nasa.gov*

- Email your question via the Internet to help@sti.nasa.gov

- Fax your question to the NASA STI Help Desk at (301) 621-0134

- Telephone the NASA STI Help Desk at (301) 621-0390

- Write to:
  NASA STI Help Desk
  NASA Center for AeroSpace Information
  7121 Standard Drive
  Hanover, MD 21076-1320

NASA / CR-2000-210297

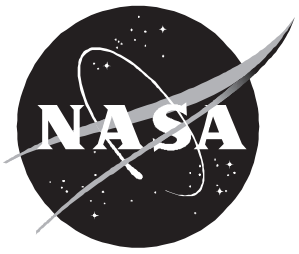

Electromagnetic Field Penetration Studies

M. D. Deshpande
NYMA, Inc., Hampton, Virginia

National Aeronautics and
Space Administration

Langley Research Center
Hampton, Virginia 23681-2199

Prepared for Langley Research Center
under Contract NAS1-96013

June 2000

Available from:

NASA Center for AeroSpace Information (CASI)
7121 Standard Drive
Hanover, MD 21076-1320
(301) 621-0390

National Technical Information Service (NTIS)
5285 Port Royal Road
Springfield, VA 22161-2171
(703) 605-6000

Contents

List of Figures

Figure 7 Electric field shielding at the center of (30. x 12. x 30.)cm3 enclosure with (10. x 3.0) cm^2aperture located at (15., 6.0) cm in z = 0 plane with three aperture modes considered.

Figure 8 Electric field shielding at the center of (30. x 12. x 30.) cm^3 enclosure with two identical apertures with (20. x 3.0) cm^2 size. Aperture one located at (15., 6., 0.0) cm, and aperture two located at (15., 6., 30.) cm.

Figure 9 Effect of higher order aperture modes on electric field shielding at the center of (30. x 12. x 30.) cm^3 enclsoure with two identical apertures of size (20. x 3.0) cm^2 . Aperture one located at (15., 6., 0.0) cm, and aperture two located at (15., 6., 30.) cm.

Figure 10 Electric field shielding of rectangular enclosure of size (30 x 12 x 30) cm^3 with two identical rectangular apertures (one on each side) of various sizes when illuminated by incident plane wave at normal incidence. Comparison with FEM/ MoM calculation.

Figure 11 Rectangular cavity with four identical apertures and illuminated by plane wave with normal incidence. All dimensions in cm.

Figure 12 Electric field shielding of rectangular cavity shown in Figure 11. Observation point (30, 6, 15) cm. Comparison with FEM/MoM calculation.

Figure 13 Geometry of B-757 aircraft configuration with cross sectional and longitudinal approximated cross section.

Figure 14(a) Closed rectangular cavity approximating a B-757 fuselage with rectangular apertures on side walls representing passenger windows.

Figure 14(b) Closed rectangular cavity approximating a B-757 fuselage with two rectangular

apertures on side walls representing passenger windows.

Figure 15 Electric field shielding (for vertical polarization) of a rectangular cavity for vertical polarization approximating fuselage of a B-757 aircraft. Two windows on each side of cavity were considered. Cavity size (3600. x 400. x 400.) cm^3, window size (25. x 35.) cm^2, window locations (1800., 200., 0.0) cm, and (1800., 200., 400.)cm, field location point (1800., 120., 200.) cm.

Figure 16 Electric field shielding (for vertical polarization) of a rectangular cavity approximating fuselage of a B-757 aircraft when two aperture modes were considered. Two windows on each side of cavity were considered. Dimensions of cavity, aperture and field point are as given in Figure 15.

Figure 17 Electric field shielding (for vertical polarization) of a rectangular cavity approximating fuselage of a B-757 aircraft when three aperture modes were considered. Two windows on each side of cavity were considered. Dimensions of cavity, aperture and field point are as given in Figure 15.

Figure 18 Electric field shielding (for horizontal polarization) of a rectangular cavity approximating fuselage of a B-757 aircraft. Two windows on each side of cavity were considered. Dimensions of cavity, aperture and their locations are as given in Figure 15.

Figure 19 Electric field amplitude at (2700., 300., 300.)cm inside a rectangular cavity of size (5400. x 600. x 600.) cm^3 illuminated by plane wave at normal incidence through rectangular windows (25. x 35.)cm^2 as a function of cavity mode index n. Other parameters: cavity mode index m = 1200, frequency = 2.87510864 GHz.

Figure 20 Electric field amplitude at (2700., 300., 300.)cm inside a rectangular cavity of size (5400. x 600. x 600.) cm^3 illuminated by plane wave at normal incidence through rectangular windows (25. x 35.)cm^2 as a function of cavity mode index m. Other parameters: cavity mode index n = 200, frequency = 2.87510864

Figure 21 Electric field amplitude at (2700., 300., 300.)cm inside a rectangular cavity of size (5400. x 600. x 600.) cm^3 illuminated by plane wave at normal incidence through rectangular windows (25. x 35.)cm^2 as a function of number of aperture modes. Other parameters: cavity mode index n = 200, m = 1200, frequency = 2.87510864 GHz GHz.

List of Symbols

a	x-dimension of rectangular cavity/approximate length of fuselage
A_{rpq}	complex modal amplitude of pq^{th} mode for aperture on $z = c$ plane (for x-directed aperture field)
b	y-dimension of rectangular cavity/approximate height of fuselage
B_{rpq}	complex modal amplitude of pq^{th} mode for aperture on $z = c$ plane (for y-directed aperture field)
c	z-dimension of cavity/approximate width of fuselage
$\vec{E}_i$	incident electric field
$\vec{E}_{apt}$	tangential aperture electric field
$\vec{E}^I(\vec{M}_{r1})$	electric field due to $\vec{M}_{r1}$ in region I
$\vec{E}^{II}(\vec{M}_r)$	electric field due to $\vec{M}_{r1}$ and $\vec{M}_{r2}$ in region II
$\vec{E}^{III}(\vec{M}_{r2})$	electric field due to $\vec{M}_{r2}$ in region III
$\vec{F}^I$	electric vector potential for region I
$\vec{F}^{II}$	electric vector potential for region II
F_x^{II}	x-component of electric vector potential
F_y^{II}	y-component of electric vector potential

$\tilde{\bar{G}}_m$	dyadic Green's function for rectangular enclosure
G_{mxx}	x-component of dyadic Green's function
G_{myy}	y-component of dyaduc Green's function
$\vec{H}_i$	incident magnetic field
H_{θ_i}	θ component of incident magnetic field
H_{ϕ_i}	ϕ component of incident magnetic field
(H_{xi}, H_{yi}, H_{zi})	x-, y-, and z- component of incident magnetic field
$\vec{H}^I(\vec{M}_{r1})$	magnetic field due to $\vec{M}_{r1}$ in region I
$\vec{H}^{II}(\vec{M}_r)$	magnetic field due to $\vec{M}_{r1}$ and $\vec{M}_{r2}$ in region II
$\vec{H}^{III}(\vec{M}_{r2})$	magnetic field due to $\vec{M}_{r2}$ in region III
$H_x^{II}, H_y^{II}, H_z^{II}$	rectangular components of vector $\vec{H}^{II}(\vec{M}_r)$
$I_{r'p'q'xi}$	coupling of testing function with x- component of incident magnetic field
$I_{r'p'q'yi}$	coupling of testing function with y- component of incident magnetic field
$\bar{\bar{I}}$	unit dyadic
j	$\sqrt{-1}$
k_0	free-space wave number
k_I	propagation constant
(k_x, k_y, k_z)	wave numbers in x-, y-, and z-directions, respectively
L_r	x-dimension of r^{th} aperture/window
$\vec{M}_{apt}$	equivalent magnetic current on aperture
$\vec{M}_{r1}$	equivalent magnetic current for apertures on $z = 0$ plane
$\vec{M}_{r2}$	equivalent magnetic current for apertures on $z = c$ plane
(m, n)	mode index numbers used for cavity modes
(p, q)	integers used for aperture modes
R	number of apertures on each side
U_{rpq}	complex modal amplitude of pq^{th} mode for aperture on $z = 0$ plane (for x-directed aperture field)

V_{rpq}	complex modal amplitude of pq^{th} mode for aperture on $z = 0$ plane
W_r	y-dimension of r^{th} aperture
$\hat{x}, \hat{y}$	unit vectors along x- and y-directions, respectively
(x_{rc}, y_{rc}, z_{rc})	coordinates of center point of r^{th} aperture
(x, y, z)	coordinates of a point in the rectangular coordinate system
$Y^{x1x1}_{rpqr'p'q'}$	mutual admittance between x-components of currents on $z = 0$ plane
$Y^{x1y1}_{rpqr'p'q'}$	mutual coupling between x- and y-components of currents on $z = 0$ plane
$Y^{x1y2}_{rpqr'p'q'}$	mutual coupling between x- component of currents on $z = 0$ plane and y-component of current on $z = c$ plane.
$Y^{x1x2}_{rpqr'p'q'}$	mutual coupling between x- component of currents on $z = 0$ plane and x-component of current on $z = c$ plane.
$Y^{y1x1}_{rpqr'p'q'}$	mutual admittance between y- and x-components of currents on $z = 0$ plane
$Y^{y1y1}_{rpqr'p'q'}$	mutual coupling between x- component of currents on $z = 0$ plane
$Y^{y1y2}_{rpqr'p'q'}$	mutual coupling between y- component of currents on $z = 0$ plane and y-component of current on $z = c$ plane.
$Y^{y1x2}_{rpqr'p'q'}$	mutual coupling between y- component of currents on $z = 0$ plane and x-component of current on $z = c$ plane.
$Y^{x2x1}_{rpqr'p'q'}$	mutual admittance between x-component of currents on $z = c$ plane and x-component of current on $z = 0$ plane
$Y^{x2y1}_{rpqr'p'q'}$	mutual coupling between x- component of currents on $z = c$ plane and y-component of current on $z = 0$ plane
$Y^{x2y2}_{rpqr'p'q'}$	mutual coupling between x- and y-components of currents on $z = c$ plane
$Y^{x2x2}_{rpqr'p'q'}$	mutual coupling between x- components of currents on $z = c$ plane
$Y^{y2x1}_{rpqr'p'q'}$	mutual admittance between y-component of currents on $z = c$ plane and x-component of current on $z = 0$ plane
$Y^{y2y1}_{rpqr'p'q'}$	mutual coupling between y- component of currents on $z = c$ plane and y-component of current on $z = 0$ plane
$Y^{y2y2}_{rpqr'p'q'}$	mutual coupling between y-components of currents on $z = c$ plane

$Y^{y2x2}_{rpqr'p'q'}$	mutual coupling between y- and x-components of currents on $z = c$ plane
Φ_{rpq}	$(p, q)^{th}$ modal function for r^{th} aperture for y-directed magnetic current
Ψ_{rpq}	$(p, q)^{th}$ modal function for r^{th} aperture for x-directed magnetic current
ϕ_{rpqy}	Fourier transform of Φ_{rpq}
ψ_{rpqx}	Fourier transform of Ψ_{rpq}
$(\hat{\theta}_i, \hat{\phi}_i)$	unit vectors in θ-and ϕ-directions
(θ_i, ϕ_i)	angle of incident plane wave
ε_{0m}	Neumann's number
ε_0	permittivity of free space
μ_0	permeability of free-space
ω	angular frequency
$\delta(\,.\,)$	Kronecker delta function
∇	gradient operator

Abstract

A numerical method is presented to determine electromagnetic shielding effectiveness of rectangular enclosure with apertures on its wall used for input and output connections, control panels, visual-access windows, ventilation panels, etc. Expressing electromagnetic fields in terms of cavity Green's function inside the enclosure and the free space Green's function outside the enclosure, integral equations with aperture tangential electric fields as unknown variables are obtained by enforcing the continuity of tangential electric and magnetic fields across the apertures. Using the Method of Moments, the integral equations are solved for unknown aperture fields. From these aperture fields, the electromagnetic fields inside a rectangular enclosure due to external electromagnetic sources are determined.

Numerical results on electric field shielding of a rectangular cavity with a thin rectangular slot obtained using the present method are compared with the results obtained using simple the transmission line technique for code validation. The present technique is applied to determine field penetration inside a Boeing -757 by approximating its passenger cabin as a rectangular cavity filled with a homogeneous medium and its passenger windows by rectangular apertures. Preliminary results for, two windows; one on each side of fuselage were considered. Numerical results on electromagnetic field penetration through passenger windows of a Boeing -757 at frequencies 26 MHz, 171-175 MHz, and 428-432 MHz are presented.

1.0 Introduction

Apertures of various sizes and shapes on a metallic enclosure are used for reasons such as input and output connections, control panels, visual-access windows, ventilation panels, etc. Since these apertures at appropriate electromagnetic (EM) frequencies behave as very efficient antennas, they also become sources of electromagnetic interference (EMI) problems for both EM emission and susceptibility. It is important to know the EM shielding effectiveness of these enclosures in presence of the apertures. The EM shielding effectiveness study may also help in locating these apertures at proper places to reduce the EM emission or improving the immunity of electronic components present inside the metallic enclosure[1]-[5]

Shielding effectiveness can be calculated using numerical or analytical methods. Numerical methods such as the Finite Difference Time Domain (FDTD) method [6], and the hybrid Finite Element/ Method of Moments [7] can model complex structures inside enclosure but often requires large computing time and memory. For electrically large size enclosures and apertures these methods , though more accurate, become difficult for designers to use to investigate effects of EM shielding on the design parameters.

Pure analytical formulations described in [3]-[5] even though provide a much faster means of calculating shielding effectiveness are based on various simplifying assumptions whose validity may be questionable at high frequencies.

In the present paper a method which is suitable for large but regular shaped enclosure and apertures is described. Using the equivalence principle as described in earlier papers [1], [2], the apertures are replaced by equivalent magnetic current sources. By matching the tangential electromagnetic fields across the apertures, coupled integro-differential equations with the magnetic currents at the apertures as an unknown variables are obtained. The coupled integro-differential

equation in conjunction with the method of moment are then solved for unknown magnetic current amplitudes. One of the advantages of the present approach is that it gives an appropriate model for EM shielding effectiveness studies and avoids some of approximations or assumptions which are made in analytical formulations to arrive at closed form formulas for EM shielding. Furthermore, by representing the magnetic current over the apertures in terms of entire domain basis functions, three to five number of unknowns per aperture are required for convergence. The present method, therefore, requires considerable less computer time compared to other numerical methods. The CPU time taken to determine EM shielding for a rectangular cavity illuminated through two rectangular apertures with three entire domain modes on each is around 23.00 seconds on a SGI Origin 2000 machine.

The remainder of this report is organized as follows. A general formulation of the problem of a rectangular cavity with a series of rectangular apertures on its broad walls which are illuminated by plane wave at normal incidence is presented in section 2. Section 2 describes: (1) use of cavity Green's function to determine electromagnetic fields scattered due to the apertures inside the cavity, (2) use of free space Green's function in plane wave spectrum form to determine scattered field outside the cavity due to apertures, (3) setting of integral equation and use of method of moments to determine matrix equation with aperture fields as unknown variables. Numerical results on electric field shielding due to horizontally and verically polarized incident waves for various sizes of rectangular cavity and rectangular apertures are given in section 3 along with earlier published data for comparison and validation. The report concludes in section 4 with remarks on the advantages and limitations of the present method. Section 4 also gives a recommendation for future work to be persued.

2.0 Formulation of Problem

Figure 1 shows a geometry of rectangular enclosure with rectangular apertures on its two opposite walls. These apertures may be used for input and output connections, control panels, visual access windows, etc. Since the rectangular apertures are very efficient electromagnetic radiators, they also act as sources of electromagnetic interference both for emission and susceptibility. The electromagnetic energy radiated by conducting wires and loops inside the enclosure may escape through these apertures and cause an interference with another electronic

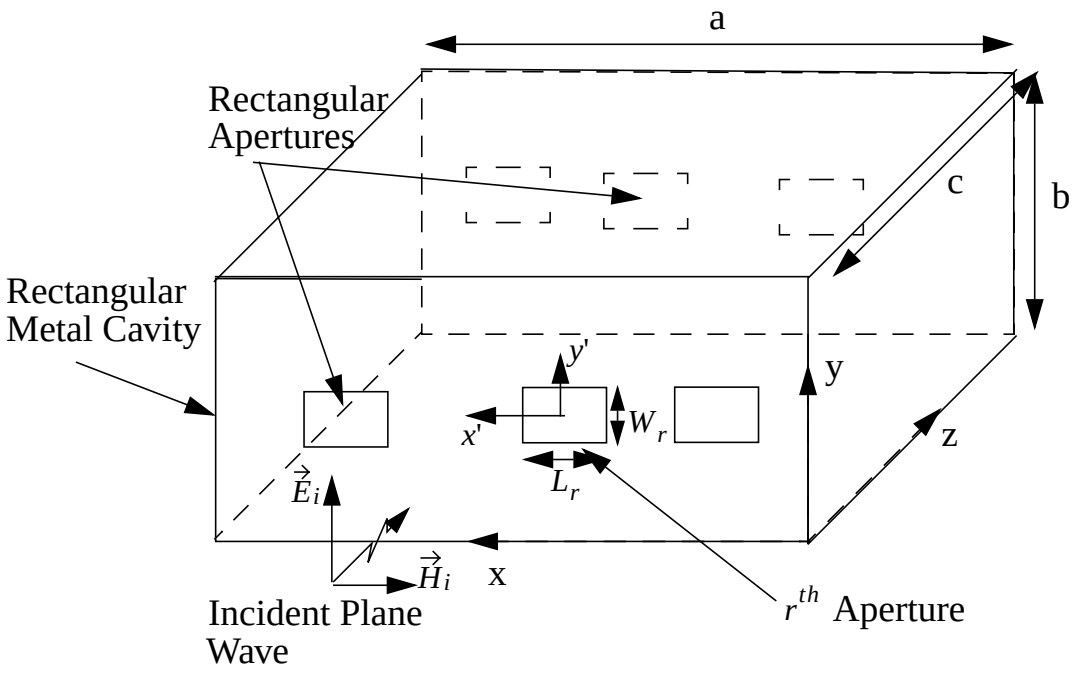

Figure 1 Geometry of rectangular enclosure with rectangular apertures illuminated by a plane wave at normal incidence.

components. The electromagnetic energy from sources outside the enclosure will get through these apertures into the enclosure and may cause interference with electronic circuits/components

present inside. In this report the latter problem is considered. To determine electromagnetic shielding effectiveness of the enclosure shown in figure 1 due to external EM radiation, a plane wave at normal incidence is assumed. This assumption is valid for worst case study. The tangential electric field induced on the apertures due to the incident field may be represented by

$$\vec{E}_{apt} = \sum_{r=1.}^{R} \sum_{p.} \sum_{q} \hat{y} U_{rpq} \sin\left(\frac{p\pi}{L_r}\left(\frac{L_r}{2} + x - x_{cr}\right)\right)\cos\left(\frac{q\pi}{W_r}\left(\frac{W_r}{2} + y - y_{cr}\right)\right)$$
$$\sum_{r=1.}^{R} \sum_{p.} \sum_{q} \hat{x} V_{rpq} \cos\left(\frac{p\pi}{L_r}\left(\frac{L_r}{2} + x - x_{cr}\right)\right)\sin\left(\frac{q\pi}{W_r}\left(\frac{W_r}{2} + y - y_{cr}\right)\right) \qquad (1)$$

where (x_{cr}, y_{cr}) are the coordinates of center of r^{th} aperture, U_{rpq} and V_{rpq} are the unknown voltages of pq^{th} mode on r^{th} aperture, W_r, L_r are the width and length of r^{th} aperture, respectively, $\hat{x}, \hat{y}$ are the unit vectors in x, y directions. In equation (1) it is assumed that there are R apertures on the $z = 0$ plane. The unknown modal amplitudes $U_{rpq} \neq 0$ and $V_{rpq} \neq 0$ for $x_{cr} - \frac{L_r}{2} \leq x \leq x_{cr} + \frac{L_r}{2}$, $y_{cr} - \frac{W_r}{2} \leq y \leq y_{cr} + \frac{W_r}{2}$, and $U_{rpq} = V_{rpq} = 0$ otherwise. Using the equivalence principle, the apertures on the plane $z = 0$ can be replaced by magnetic currents given by

$$\vec{M}_{apt} = \sum_{r=1}^{R} \sum_{p} \sum_{q} V_{rpq}(-\hat{y}\Phi_{rpqy}) + \sum_{r=1}^{R} \sum_{p} \sum_{q} U_{rpq}\hat{x}\Psi_{rpqx} = \sum_{r=1}^{R} \vec{M}_{r1} \qquad (2)$$

Likewise the apertures on the plane $z = c$ can be replaced by equivalent magnetic currents given by

$$\vec{M}_{apt} = \sum_{r=1}^{R} \sum_{pq} A_{rpq}\hat{y}\Phi_{rpqy} + \sum_{r=1}^{R} \sum_{pq} B_{rpq}(-\hat{x}\Psi_{rpqx}) = \sum_{r=1}^{R} \vec{M}_{r2} \qquad (3)$$

where

$$\Phi_{rpqy} = \cos\left(\frac{p\pi}{L_r}\left(\frac{L_r}{2} + x - x_{cr}\right)\right)\sin\left(\frac{q\pi}{W_r}\left(\frac{W_r}{2} + y - y_{cr}\right)\right)$$

$$\Psi_{rpqx} = \sin\left(\frac{p\pi}{L_r}\left(\frac{L_r}{2} + x - x_{cr}\right)\right)\cos\left(\frac{q\pi}{W_r}\left(\frac{W_r}{2} + y - y_{cr}\right)\right)$$

and A_{rpq}, B_{rpq} are the unknown modal amplitudes corresponding to the apertures on $z = c$ plane and they satisfiy $A_{rpq} \neq 0$, and $B_{rpq} \neq 0$ for $x_{cr} - \frac{L_r}{2} \leq x \leq x_{cr} + \frac{L_r}{2}$, $y_{cr} - \frac{W_r}{2} \leq y \leq y_{cr} + \frac{W_r}{2}$, and $A_{rpq} = B_{rpq} = 0$ otherwise. The problem of EM coupling to a rectangular enclosure through apertures therefore can be split into internal and external regions as shown in Figure 2. Assuming the $z = 0$ and $z = c$ planes are infinite, the entire problem can be split into three regions: region I for $z \leq 0$, region II for $0 \leq z \leq c$, and region III for $z \geq c$. It should be noted that because of the presence of the infinite ground planes at $z = 0$ and $z = c$, the apertures on the $z = 0$ plane do not couple to the apertures on the $z = c$ externally.

The internal problem consists of a rectangular volume enclosed by the enclosure and illuminated by various equivalent magnetic current sources. The external problem consists of magnetic current sources backed by infinite ground plane for each wall of the rectangular enclosure. The unknown amplitudes V_{rpq}, U_{rpq}, A_{rpq}, and B_{rpq} appearing in (2) and (3) are determined by setting up coupled integral equations. The expressions for the EM fields required to form integral equation are determined in the following sections.

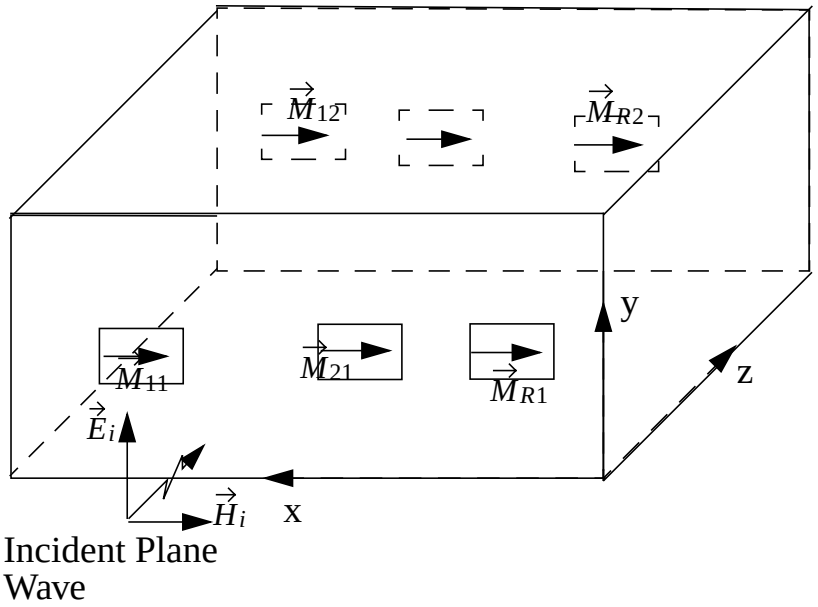

Figure 2 Geometry of equivalent problem with apertures replaced by magnetic current sources.

2.1 Electromagnetic Field Outside Enclosure

The total electromagnetic field outside the enclosure is obtained by superposition of the field due to incident wave and the scattered field due to apertures. In the following sections the EM field due to incident wave and the scattered field due to aperture are determined.

2.1.1 Electromagnetic Field Due to Incident Wave

The incident field with a time variation of $e^{j\omega t}$ may be written as

$$\vec{H}_i = (\hat{\theta}_i H_{\theta_i} + \hat{\phi}_i H_{\phi_i}) e^{-\vec{k}_i \bullet \vec{r}}$$

$$= (\hat{\theta}_i |H_i| \cos(\alpha_0) + \hat{\phi}_i |H_i| \sin(\alpha_0)) e^{-\vec{k}_i \bullet \vec{r}} \qquad (4)$$

where $\vec{k}_i \bullet \vec{r} = -k_0 \sin(\theta_i)(x\cos(\phi_i) + y\sin(\phi_i)) - zk_0\cos(\theta_i)$, k_0 is the free-space wave number, and (θ_i, ϕ_i) are the angle of incident plane wave. From equation (4), the x-, -y, and z-components of the incident magnetic field may be written, respectively as

$$H_{xi} = H_{\theta_i}\cos(\theta_i)\cos(\phi_i) - H_{\phi_i}\sin(\phi_i) \tag{5}$$

$$H_{yi} = H_{\theta_i}\cos(\theta_i)\sin((\phi_i) + H_{\phi_i}\cos(\phi_i)) \tag{6}$$

$$H_{zi} = -H_{\theta_i}\sin(\theta_i) \tag{7}$$

For normal incidence, with $\alpha_0 = 0$, $\theta_i = 0$, and $\phi_i = 0$, the incident field in the $z = 0$ is given by $H_{xi} = \left|\vec{H}_i\right|$, $H_{yi} = 0$, and $H_{zi} = 0$.

2.1.2 Electromagnetic Field Scattered due to Apertures:

Consider the r^{th} aperture on the $z = 0$ plane, the EM field scattered due to $\vec{M}_{r1}$ can be obtained from [8]

$$\vec{E}^I(\vec{M}_r) = \frac{-1}{\varepsilon_0}\nabla\times\vec{F}^I \tag{8}$$

$$\vec{H}^I(\vec{M}_r) = \frac{-j\omega}{k_0^2}(k_0^2\vec{F}^I + \nabla(\nabla\bullet\vec{F}^I)) \tag{9}$$

where the electric vector potential $\vec{F}^I$ is given by

$$\vec{F}^I = \frac{\varepsilon_0}{4\pi}\int\limits_{Apt}\int 2\vec{M}_r\frac{e^{-jk_0\left|\vec{r}-\vec{r}'\right|}}{\left|\vec{r}-\vec{r}'\right|}ds \tag{10}$$

The factor 2 in equation (9) is considered to take into account the image. In deriving (9) it is assumed that the $z = 0$ plane is an infinite. Expressing $\frac{e^{-jk_0\left|\vec{r}-\vec{r}'\right|}}{\left|\vec{r}-\vec{r}'\right|}$ in terms of plane waves [8] as

$$\frac{e^{-jk_0|\vec{r}-\vec{r}'|}}{|\vec{r}-\vec{r}'|} = \frac{1}{2\pi j}\int_{-\infty}^{\infty}\int_{-\infty}^{\infty}\frac{e^{-jk_z|(z-z')|}}{k_z}e^{jk_x(x-x')+jk_y(y-y')}dk_xdk_y$$

the electric vector potential can be written in form

$$\vec{F}^I = \frac{\varepsilon_0}{4\pi^2}\int_{-\infty}^{\infty}\int_{-\infty}^{\infty}\left(\frac{e^{-jk_z|(z-z')|}}{jk_z}\vec{m}_r\right)e^{jk_xx+jk_yy}dk_xdk_y \tag{11}$$

where $\vec{m}_{r1} = \int\int_{Apt}\vec{M}_{r1}e^{jk_x(-x')+jk_y(-y')}ds$

$k_z = \sqrt{k_0^2-k_x^2-k_y^2}$ for $k_0^2 \geq k_x^2+k_y^2$ and

$= -j\sqrt{k_x^2+k_y^2-k_0^2}$ for $k_0^2 \leq (k_x^2+k_y^2)$

Substituting (11) in equations (8) and (9), the scattered electromagnetic field dueto the r^{th} aperture is obtained. Superposition of the scattered electromagnetic field due to all apertures on the $z = 0$ gives the total scattered field as

$$E_x^I = \sum_{r=1}^{R}\sum_{p,q}\frac{-V_{rpq}}{4\pi^2}\int_{-\infty}^{\infty}\int_{-\infty}^{\infty}e^{-jk_z|(z-z')|}\phi_{rpqy}e^{jk_xx+jk_yy}dk_xdk_y \tag{12}$$

$$E_y^I = \sum_{r=1}^{R}\sum_{pq}\frac{-U_{rpq}}{4\pi^2}\int_{-\infty}^{\infty}\int_{-\infty}^{\infty}e^{-jk_z|(z-z')|}\psi_{rpqx}e^{jk_xx+jk_yy}dk_xdk_y \tag{13}$$

$$E_z^I = \sum_{r=1}^{R}\sum_{pq}\frac{-1}{4\pi^2}\int_{-\infty}^{\infty}\int_{-\infty}^{\infty}e^{-jk_z|(z-z')|}\frac{(V_{rpq}\phi_{rpqy}k_x+U_{rpq}\psi_{rpqx}k_y)}{k_z}e^{jk_xx+jk_yy}dk_xdk_y \tag{14}$$

$$H_x^I = \sum_{r=1}^{R}\sum_{pq}\frac{\omega\varepsilon_0U_{rpq}}{4\pi^2k_0^2}\int_{-\infty}^{\infty}\int_{-\infty}^{\infty}e^{-jk_z|(z-z')|}\psi_{rpqx}\frac{(k_0^2-k_x^2)}{k_z}e^{jk_xx+jk_yy}dk_xdk_y$$

$$+\sum_{r=1}^{R}\sum_{pq}\frac{-\omega\varepsilon_0 V_{rpq}}{4\pi^2 k_0^2}\int_{-\infty}^{\infty}\int_{-\infty}^{\infty}e^{-jk_z|(z-z')|}\phi_{rpqy}\frac{(-k_x k_y)}{k_z}e^{jk_x x+jk_y y}dk_x dk_y \tag{15}$$

$$H_y^I=\sum_{r=1}^{R}\sum_{pq}\frac{-\omega\varepsilon_0 V_{rpq}}{4\pi^2 k_0^2}\int_{-\infty}^{\infty}\int_{-\infty}^{\infty}e^{-jk_z|(z-z')|}\phi_{rpqy}\frac{(k_0^2-k_y^2)}{k_z}e^{jk_x x+jk_y y}dk_x dk_y$$

$$+\sum_{r=1}^{R}\sum_{pq}\frac{\omega\varepsilon_0 U_{rpq}}{4\pi^2 k_0^2}\int_{-\infty}^{\infty}\int_{-\infty}^{\infty}e^{-jk_z|(z-z')|}\psi_{rpqx}\frac{(-k_x k_y)}{k_z}e^{jk_x x+jk_y y}dk_x dk_y \tag{16}$$

$$H_z^I=\sum_{r=1}^{R}\sum_{pq}\frac{-\omega\varepsilon_0}{4\pi^2 k_0^2}\int_{-\infty}^{\infty}\int_{-\infty}^{\infty}e^{-jk_z|(z-z')|}(U_{rpq}\psi_{rpqx}k_x-V_{rpq}\phi_{rpqy}k_y)e^{jk_x x+jk_y y}dk_x dk_y \tag{17}$$

In expressions (12)-(17) ϕ_{rpqy} is the Fourier transform of Φ_{rpqy} and ψ_{rpqx} is the Fourier transform of Ψ_{rpqx}. The expressions for ϕ_{rpqy} and ψ_{rpqx} are given in Appendix III.

Consider the r^{th} aperture on the $z = c$ plane, the EM field scattered due to $\vec{M}_{r2}$ can be obtained following the same procedure

$$E_x^{III}=\sum_{r=1}^{R}\sum_{p,\,q}\frac{A_{rpq}}{4\pi^2}\int_{-\infty}^{\infty}\int_{-\infty}^{\infty}e^{-jk_z|(z-z')|}\phi_{rpqy}e^{jk_x x+jk_y y}dk_x dk_y \tag{18}$$

$$E_y^{III}=\sum_{r=1}^{R}\sum_{pq}\frac{B_{rpq}}{4\pi^2}\int_{-\infty}^{\infty}\int_{-\infty}^{\infty}e^{-jk_z|(z-z')|}\psi_{rpqx}e^{jk_x x+jk_y y}dk_x dk_y \tag{19}$$

$$E_z^{III}=\sum_{r=1}^{R}\sum_{pq}\frac{1}{4\pi^2}\int_{-\infty}^{\infty}\int_{-\infty}^{\infty}e^{-jk_z|(z-z')|}\frac{(A_{rpq}\phi_{rpqy}k_x+B_{rpq}\psi_{rpqx}k_y)}{k_z}e^{jk_x x+jk_y y}dk_x dk_y \tag{20}$$

$$H_x^{III}=\sum_{r=1}^{R}\sum_{pq}\frac{-\omega\varepsilon_0 B_{rpq}}{4\pi^2 k_0^2}\int_{-\infty}^{\infty}\int_{-\infty}^{\infty}e^{-jk_z|(z-z')|}\psi_{rpqx}\frac{(k_0^2-k_x^2)}{k_z}e^{jk_x x+jk_y y}dk_x dk_y$$

$$+\sum_{r=1}^{R}\sum_{pq}\frac{\omega\varepsilon_0 A_{rpq}}{4\pi^2 k_0^2}\int_{-\infty}^{\infty}\int_{-\infty}^{\infty}e^{-jk_z|(z-z')|}\phi_{rpqy}\frac{(-k_x k_y)}{k_z}e^{jk_x x+jk_y y}dk_x dk_y \tag{21}$$

$$H_y^{III}=\sum_{r=1}^{R}\sum_{pq}\frac{\omega\varepsilon_0 A_{rpq}}{4\pi^2 k_0^2}\int_{-\infty}^{\infty}\int_{-\infty}^{\infty}e^{-jk_z|(z-z')|}\phi_{rpqy}\frac{(k_0^2-k_y^2)}{k_z}e^{jk_x x+jk_y y}dk_x dk_y$$

$$+\sum_{r=1}^{R}\sum_{pq}\frac{-\omega\varepsilon_0 B_{rpq}}{4\pi^2 k_0^2}\int_{-\infty}^{\infty}\int_{-\infty}^{\infty}e^{-jk_z|(z-z')|}\psi_{rpqx}\frac{(-k_x k_y)}{k_z}e^{jk_x x+jk_y y}dk_x dk_y \tag{22}$$

$$H_z^{III}=\sum_{r=1}^{R}\sum_{pq}\frac{-\omega\varepsilon_0}{4\pi^2 k_0^2}\int_{-\infty}^{\infty}\int_{-\infty}^{\infty}e^{-jk_z|(z-z')|}(B_{rpq}\psi_{rpqx}k_x-A_{rpq}\phi_{rpqy}k_y)e^{jk_x x+jk_y y}dk_x dk_y.$$

2.2 Electromagnetic Field Inside Enclosure

The equivalent magnetic currents, present on the apertures of an enclosure radiate electromagnetic fields inside the enclosure. The total EM field at any point inside is obtained by a superposition of fields due to each equivalent magnetic current source. Consider the r^{th} aperture, the electromagnetic field inside the enclosure due to the r^{th} aperture is obtained from

$$\vec{E}^{II}=-\frac{1}{\varepsilon_0}\nabla\times\vec{F}^{II} \tag{23}$$

$$\vec{H}^{II}=\frac{-j\omega}{k_0^2}(k_0^2\vec{F}^{II}+\nabla\nabla\bullet\vec{F}^{II}) \tag{24}$$

where the assumed variation $e^{j\omega t}$ has been suppressed. The electric vector potential appearing in (23) and (24) satifies the inhomogeneous wave equation

$$\nabla^2\vec{F}^{II}(x,y,z)+k_0^2\vec{F}^{II}=-\varepsilon_0\vec{M}_r(x,y,z) \tag{25}$$

If $\tilde{G}_m(x,y,z/x',y',z')$ is the dyadic Green's function for the rectangular enclosure for a unit dyad $\overset{\leftrightarrow}{I}(x',y',z')=\hat{x}\hat{x}+\hat{y}\hat{y}+\hat{z}\hat{z}$ inside the enclosure, then the electric vector potential $\vec{F}^{II}$ can be written in the form

$$\vec{F}^{II}(x, y, z) = \iint_{Source} \tilde{G}_m(x, y, z/x', y', z') \bullet \vec{M}_r(x', y', z')dx'dy'dz' \tag{26}$$

Substitution of (26) in (25) yields

$$\nabla^2\tilde{G}_m + k_0^2\tilde{G}_m = -\varepsilon_0\hat{\vec{I}}\delta(x-x')\delta(y-y')\delta(z-z') \tag{27}$$

Since the apertures are in the xy plane and $\vec{M}_r$ can have both the x- and y-directions, $\hat{\vec{I}}(x', y', z') = \hat{x}\hat{x} + \hat{y}\hat{y}$, hence equation (27) can be written in component forms as

$$\nabla^2 G_{mxx} + k_0^2 G_{mxx} = -\varepsilon_0\delta(x-x')\delta(y-y')\delta(z-z') \tag{28}$$

$$\nabla^2 G_{myy} + k_0^2 G_{myy} = -\varepsilon_0\delta(x-x')\delta(y-y')\delta(z-z') \tag{29}$$

2.2.1 Electromagnetic Fields Scattered Due to Apertures on $z = 0$ Plane

Considering the x-component of the magentic current and using the proper boundary conditions, the solution of equation (28) can be written as

$$G_{xx} = \sum_{m,n}^{\infty} \frac{\varepsilon_0\varepsilon_{0m}\varepsilon_{0n}}{k_I}\frac{}{ab}\sin\left(\frac{m\pi x'}{a}\right)\cos\left(\frac{n\pi y'}{b}\right)\frac{\cos(k_I(z-c))}{\sin(k_I c)}\sin\left(\frac{m\pi x}{a}\right)\cos\left(\frac{n\pi y}{b}\right)\delta(z') \tag{30}$$

for the aperture located in the $z = 0$ plane. In expressions (30) $\sum_{m,n}^{\infty}(.) = \sum_{m=0}^{\infty}\sum_{n=0}^{\infty}(.)$,

$k_I = \sqrt{k_0^2 - \left(\frac{m\pi}{a}\right)^2 - \left(\frac{n\pi}{b}\right)^2}$ for $k_0^2 \geq \left(\frac{m\pi}{a}\right)^2 + \left(\frac{n\pi}{b}\right)^2$ and $k_I = -j\sqrt{\left(\frac{m\pi}{a}\right)^2 + \left(\frac{n\pi}{b}\right)^2 - k_0^2}$ for $k_0^2 \leq \left(\frac{m\pi}{a}\right)^2 + \left(\frac{n\pi}{b}\right)^2$, $\varepsilon_{0m} = 1$ for $m = 0$ and $\varepsilon_{0m} = 2$ for $m \neq 0$. Substituting (30) into (26) the electric vector potential $\vec{F}^{IIx0}$ due to the x-component of $\vec{M}_r$ on the plane $z = 0$ is obtained as

$$F_x^{IIx0} = \sum_{m,\,n}^{\infty} \frac{-\varepsilon_0}{k_I} \frac{\varepsilon_{0m}\varepsilon_{0n}}{ab\sin(k_I c)} \cos(k_I(z-c)) \sin\left(\frac{m\pi x}{a}\right) \cos\left(\frac{n\pi y}{b}\right)$$
$$\iint_q \left((\vec{M}_r(x', y', 0) \bullet \hat{x}) \sin\left(\frac{m\pi x'}{a}\right) \cos\left(\frac{n\pi y'}{b}\right) \right) dx'dy' \qquad (31)$$

The total electric vector potential due to all the apertures is then obtained by superposition as

$$F_x^{IIx0} = \sum_{r\,=\,1}^{R} \sum_{p,\,q} U_{rpq} \sum_{m,\,n}^{\infty} \frac{-\varepsilon_0}{k_I} \frac{\varepsilon_{0m}\varepsilon_{0n}}{ab\sin(k_I c)} \cos(k_I(z-c)) \sin\left(\frac{m\pi x}{a}\right) \cos\left(\frac{n\pi y}{b}\right)$$
$$\iint_q (\vec{\Psi}_{rpq}(x', y') \bullet \hat{x}) \sin\left(\frac{m\pi x'}{a}\right) \cos\left(\frac{n\pi y'}{b}\right) dx'dy' \qquad (32)$$

Since $\vec{\Psi}_{rpq}(x', y') = \hat{x}\Psi_{rpqx}(x', y')$, expression (32) can be written in component form as

$$F_x^{IIx0} = \sum_{r\,=\,1}^{R} \sum_{p,\,q} U_{rqp} \sum_{m,\,n}^{\infty} \frac{-\varepsilon_0}{k_I} \frac{\varepsilon_{0m}\varepsilon_{0n}}{ab\sin(k_I c)} \cos(k_I(z-c)) \sin\left(\frac{m\pi x}{a}\right) \cos\left(\frac{n\pi y}{b}\right)$$
$$\iint_q \Psi_{rpqx}(x', y') \sin\left(\frac{m\pi x'}{a}\right) \cos\left(\frac{n\pi y'}{b}\right) dx'dy' \qquad (33)$$

The total magnetic field inside the enclosure is then obtained from (24) and (33) as

$$H_x^{IIx0} = \frac{-j\omega}{k_0^2} \sum_{r\,=\,1}^{R} \sum_{p,\,q} U_{rpq} \sum_{m,\,n}^{\infty} \frac{-\varepsilon_0}{k_I} \frac{\varepsilon_{0m}\varepsilon_{0n}}{ab\sin(k_I c)} \left(k_0^2 - \left(\frac{m\pi}{a}\right)^2\right) \sin\left(\frac{m\pi x}{a}\right) \cos\left(\frac{n\pi y}{b}\right)$$
$$\cos(k_I(z-c)) I_{rpqmnx} \qquad (34)$$

$$H_y^{IIx0} = \frac{-j\omega}{k_0^2} \sum_{r\,=\,1}^{R} \sum_{p,\,q} U_{rpq} \sum_{m,\,n}^{\infty} \frac{-\varepsilon_0}{k_I} \frac{\varepsilon_{0m}\varepsilon_{0n}}{ab\sin(k_I c)} \frac{m\pi}{a} \left(-\frac{n\pi}{b}\right) \cos\left(\frac{m\pi x}{a}\right) \sin\left(\frac{n\pi y}{b}\right)$$
$$\cos(k_I(z-c)) I_{rpqmnx} \qquad (35)$$

$$H_z^{IIx0} = \frac{-j\omega}{k_0^2} \sum_{r\,=\,1}^{R} \sum_{p,\,q} U_{rpq} \sum_{m,\,n}^{\infty} \frac{-\varepsilon_0}{k_I} \frac{\varepsilon_{0m}\varepsilon_{0n}}{ab\sin(k_I c)} \frac{m\pi}{a} (-k_I) \cos\left(\frac{m\pi x}{a}\right) \cos\left(\frac{n\pi y}{b}\right)$$
$$\sin(k_I(z-c)) I_{rpqmnx} \qquad (36)$$

In (34)-(36), I_{rpqmnx} is equal to $\iint_q \Psi_{rpqx}(x', y') \sin\left(\frac{m\pi x'}{a}\right) \cos\left(\frac{n\pi y'}{b}\right) dx' dy'$ and can be expressed in closed form (see Appendix I).

Likewise, considering the y-component of the magnetic current and using the proper boundary conditions, the solution of equation (29) can be written as

$$G_{myy} = \sum_{m,\,n}^{\infty} \frac{-\varepsilon_0}{k_I} \frac{\varepsilon_{0m}\varepsilon_{0n}}{ab} \cos\left(\frac{m\pi x'}{a}\right) \sin\left(\frac{n\pi y'}{b}\right) \frac{\cos(k_I(z-c))}{\sin(k_I c)} \cos\left(\frac{m\pi x}{a}\right) \sin\left(\frac{n\pi y}{b}\right) \delta(z') \qquad (37)$$

for the aperture located in the $z = 0$ plane Substituting (37) into (26) the electric vector potential $\vec{F}^{IIy0}$ due to the y-component of $\vec{M}_r$ due to apertures in the $z = 0$ plane is obtained as

$$F_y^{IIy0} = \sum_{m,\,n}^{\infty} \frac{-\varepsilon_0}{k_I} \frac{\varepsilon_{0m}\varepsilon_{0n}}{ab \sin(k_I c)} \cos(k_I(z-c)) \cos\left(\frac{m\pi x}{a}\right) \sin\left(\frac{n\pi y}{b}\right) \iint_q \left((\vec{M}_r(x', y') \bullet \hat{y}) \cos\left(\frac{m\pi x'}{a}\right) \sin\left(\frac{n\pi y'}{b}\right) \right) dx' dy' \qquad (38)$$

The total electric vector potential due to all apertures on $z = 0$ is then obtained by superposition as

$$F_y^{IIy0} = \sum_{r=1}^{R} \sum_{p,\,q} V_{rpq} \sum_{m,\,n}^{\infty} \frac{-\varepsilon_0}{k_I} \frac{\varepsilon_{0m}\varepsilon_{0n}}{ab \sin(k_I c)} \cos(k_I(z-c)) \cos\left(\frac{m\pi x}{a}\right) \sin\left(\frac{n\pi y}{b}\right) \iint_q (\vec{\Phi}_{rpq}(x', y') \bullet \hat{y}) \cos\left(\frac{m\pi x'}{a}\right) \sin\left(\frac{n\pi y'}{b}\right) dx' dy' \qquad (39)$$

Since $\vec{\Phi}_{rqp}(x', y') = -\hat{y}\Phi_{rqpy}(x', y')$, expression (39) can be written as

$$F_y^{IIy0} = \sum_{r=1}^{R} \sum_{p,\,q} -V_{rpq} \sum_{m,\,n}^{\infty} \frac{-\varepsilon_0}{k_I} \frac{\varepsilon_{0m}\varepsilon_{0n}}{ab \sin(k_I c)} \cos(k_I(z-c)) \cos\left(\frac{m\pi x}{a}\right) \sin\left(\frac{n\pi y}{b}\right) \iint_q \Phi_{rpqy}(x', y') \cos\left(\frac{m\pi x'}{a}\right) \sin\left(\frac{n\pi y'}{b}\right) dx' dy' \qquad (40)$$

The total magnetic field inside the enclosure is then obtained from (24) and (40) as

$$H_x^{IIy0} = \frac{-j\omega}{k_0^2}\sum_{r=1}^{R}\sum_{p,q} -V_{rpq}\sum_{m,n}^{\infty}\frac{-\varepsilon_0}{k_I}\frac{\varepsilon_{0m}\varepsilon_{0n}}{ab\sin(k_I c)}\left(-\frac{m\pi}{a}\right)\frac{n\pi}{b}\sin\left(\frac{m\pi x}{a}\right)\cos\left(\frac{n\pi y}{b}\right)$$
$$\cos(k_I(z-c))I_{rpqmny} \tag{41}$$

$$H_y^{IIy0} = \frac{-j\omega}{k_0^2}\sum_{r=1}^{R}\sum_{p,q} -V_{rpq}\sum_{m,n}^{\infty}\frac{-\varepsilon_0}{k_I}\frac{\varepsilon_{0m}\varepsilon_{0n}}{ab\sin(k_I c)}\left(k_0^2-\left(\frac{n\pi}{b}\right)^2\right)\cos\left(\frac{m\pi x}{a}\right)\sin\left(\frac{n\pi y}{b}\right)$$
$$\cos(k_I(z-c))I_{rpqmny} \tag{42}$$

$$H_z^{IIy0} = \frac{-j\omega}{k_0^2}\sum_{r=1}^{R}\sum_{p,q} -V_{rpq}\sum_{m,n}^{\infty}\frac{-\varepsilon_0}{k_I}\frac{\varepsilon_{0m}\varepsilon_{0n}}{ab\sin(k_I c)}\frac{n\pi}{b}(-k_I)\cos\left(\frac{m\pi x}{a}\right)\cos\left(\frac{n\pi y}{b}\right)$$
$$\sin(k_I(z-c))I_{rpqmny} \tag{43}$$

where I_{rpqmny} appearing in (41)-(43) is equal to $\iint_q \Phi_{rpqy}(x', y')\cos\left(\frac{m\pi x'}{a}\right)\sin\left(\frac{n\pi y'}{b}\right)dx'dy'$ and can be expressed in closed form (see Appendix II).

2.2.2 Electromagnetic Fields Scattered Due to Apertures on $z = c$ Plane

Considering the x-component of the magnetic current and using the proper boundary conditions, the solution of equation (28) can be written as

$$G_{xx} = \sum_{m,n}^{\infty}\frac{-\varepsilon_0}{k_I}\frac{\varepsilon_{0m}\varepsilon_{0n}}{ab}\sin\left(\frac{m\pi x'}{a}\right)\cos\left(\frac{n\pi y'}{b}\right)\frac{\cos(k_I z)}{\sin(k_I c)}\sin\left(\frac{m\pi x}{a}\right)\cos\left(\frac{n\pi y}{b}\right)\delta(z-c) \tag{44}$$

for the aperture located in the $z = c$ plane. Substituting (44) into (26) the electric vector potential $\vec{F}^{IIxc}$ due to the x-component of $\vec{M}_r$ on the plane $z = c$ is obtained as

$$F_x^{IIxc} = \sum_{m,n}^{\infty}\frac{-\varepsilon_0}{k_I}\frac{\varepsilon_{0m}\varepsilon_{0n}}{ab\sin(k_I c)}\cos(k_I z)\sin\left(\frac{m\pi x}{a}\right)\cos\left(\frac{n\pi y}{b}\right)$$
$$\iint_q\left((\vec{M}_r(x', y', c)\bullet\hat{x})\sin\left(\frac{m\pi x'}{a}\right)\cos\left(\frac{n\pi y'}{b}\right)\right)dx'dy' \tag{45}$$

The total electric vector potential due to all apertures is then obtained by superposition as

$$F_x^{IIxc} = \sum_{r=1}^{R}\sum_{p,q} B_{rpq}\sum_{m,n}^{\infty}\frac{-\varepsilon_0}{k_I}\frac{\varepsilon_{0m}\varepsilon_{0n}}{ab\sin(k_I c)}\cos(k_I z)\sin\left(\frac{m\pi x}{a}\right)\cos\left(\frac{n\pi y}{b}\right)$$

$$\iint_q (\vec{\Psi}_{rpq}(x', y', c) \bullet \hat{x}) \sin\left(\frac{m\pi x'}{a}\right) \cos\left(\frac{n\pi y'}{b}\right) dx' dy' \tag{46}$$

Since $\vec{\Psi}_{rpq}(x', y', c) = -\hat{x}\Psi_{rpqx}(x', y')$, expression (46) can be written in component form as

$$F_x^{IIxc} = \sum_{r=1}^{R} \sum_{p,q} (-B_{rqp}) \sum_{m,n}^{\infty} \frac{-\varepsilon_0}{k_I} \frac{\varepsilon_{0m}\varepsilon_{0n}}{ab\sin(k_I c)} \cos(k_I z) \sin\left(\frac{m\pi x}{a}\right) \cos\left(\frac{n\pi y}{b}\right)$$
$$\iint_r \Psi_{rpqx}(x', y') \sin\left(\frac{m\pi x'}{a}\right) \cos\left(\frac{n\pi y'}{b}\right) dx' dy' \tag{47}$$

The total magnetic field inside the enclosure is then obtained from (24) and (47) as

$$H_x^{IIxc} = \frac{-j\omega}{k_0^2} \sum_{r=1}^{R} \sum_{p,q} (-B_{rqp}) \sum_{m,n}^{\infty} \frac{-\varepsilon_0}{k_I} \frac{\varepsilon_{0m}\varepsilon_{0n}}{ab\sin(k_I c)} \left(k_0^2 - \left(\frac{m\pi}{a}\right)^2\right) \sin\left(\frac{m\pi x}{a}\right) \cos\left(\frac{n\pi y}{b}\right)$$
$$\cos(k_I z) I_{rpqmnx} \tag{48}$$

$$H_y^{IIxc} = \frac{-j\omega}{k_0^2} \sum_{r=1}^{R} \sum_{p,q} (-B_{rqp}) \sum_{m,n}^{\infty} \frac{-\varepsilon_0}{k_I} \frac{\varepsilon_{0m}\varepsilon_{0n}}{ab\sin(k_I c)} \frac{m\pi}{a} \left(-\frac{n\pi}{b}\right) \cos\left(\frac{m\pi x}{a}\right) \sin\left(\frac{n\pi y}{b}\right)$$
$$\cos(k_I z) I_{rpqmnx} \tag{49}$$

$$H_z^{IIxc} = \frac{-j\omega}{k_0^2} \sum_{r=1}^{R} \sum_{p,q} (-B_{rqp}) \sum_{m,n}^{\infty} \frac{-\varepsilon_0}{k_I} \frac{\varepsilon_{0m}\varepsilon_{0n}}{ab\sin(k_I c)} \frac{m\pi}{a} (-k_I) \cos\left(\frac{m\pi x}{a}\right) \cos\left(\frac{n\pi y}{b}\right)$$
$$\sin(k_I z) I_{rpqmnx} \tag{50}$$

Considering the y-component of the magnetic current and using the proper boundary conditions, the solution of equation (29) can be written as

$$G_{myy} = \sum_{m,n}^{\infty} \frac{-\varepsilon_0}{k_I} \frac{\varepsilon_{0m}\varepsilon_{0n}}{ab} \cos\left(\frac{m\pi x'}{a}\right) \sin\left(\frac{n\pi y'}{b}\right) \frac{\cos(k_I z)}{\sin(k_I c)} \cos\left(\frac{m\pi x}{a}\right) \sin\left(\frac{n\pi y}{b}\right) \delta(z - c) \tag{51}$$

for the aperture located in the $z = c$ plane. Substituting (51) into (26) the electric vector potential $\vec{F}^{IIyc}$ due to the y-component of $\vec{M}_r$ due to apertures in the $z = c$ plane is obtained as

$$F_y^{IIyc} = \sum_{m,n}^{\infty} \frac{-\varepsilon_0}{k_I} \frac{\varepsilon_{0m}\varepsilon_{0n}}{ab\sin(k_I c)} \cos(k_I z) \cos\left(\frac{m\pi x}{a}\right) \sin\left(\frac{n\pi y}{b}\right)$$

$$\iint_r \left((\vec{M}_r(x', y', c) \bullet \hat{y}) \cos\left(\frac{m\pi x'}{a}\right) \sin\left(\frac{n\pi y'}{b}\right) \right) dx'dy' \tag{52}$$

The total electric vector potential due to all apertures on $z = c$ is then obtained by superposition as

$$F_y^{IIyc} = \sum_{r=1}^{R} \sum_{p,q} A_{rpq} \sum_{m,n}^{\infty} \frac{-\varepsilon_0}{k_I} \frac{\varepsilon_{0m}\varepsilon_{0n}}{ab \sin(k_I c)} \cos(k_I z) \cos\left(\frac{m\pi x}{a}\right) \sin\left(\frac{n\pi y}{b}\right)$$
$$\iint_r (\vec{\Phi}_{rpq}(x', y', c) \bullet \hat{y}) \cos\left(\frac{m\pi x'}{a}\right) \sin\left(\frac{n\pi y'}{b}\right) dx'dy' \tag{53}$$

Since $\vec{\Phi}_{rqp}(x', y', c) = \hat{y}\Phi_{rqpy}(x', y')$, expression (53) can be written in component form as

$$F_y^{IIyc} = \sum_{r=1}^{R} \sum_{p,q} A_{rpq} \sum_{m,n}^{\infty} \frac{-\varepsilon_0}{k_I} \frac{\varepsilon_{0m}\varepsilon_{0n}}{ab \sin(k_I c)} \cos(k_I z) \cos\left(\frac{m\pi x}{a}\right) \sin\left(\frac{n\pi y}{b}\right)$$
$$\iint_r \Phi_{rpqy}(x', y') \cos\left(\frac{m\pi x'}{a}\right) \sin\left(\frac{n\pi y'}{b}\right) dx'dy' \tag{54}$$

The total magnetic field inside the enclosure is then obtained from (24) and (54) as

$$H_x^{IIyc} = \frac{-j\omega}{k_0^2} \sum_{r=1}^{R} \sum_{p,q} A_{rpq} \sum_{m,n}^{\infty} \frac{-\varepsilon_0}{k_I} \frac{\varepsilon_{0m}\varepsilon_{0n}}{ab \sin(k_I c)} \left(-\frac{m\pi}{a}\right) \frac{n\pi}{b} \sin\left(\frac{m\pi x}{a}\right) \cos\left(\frac{n\pi y}{b}\right)$$
$$\cos(k_I z) I_{rpqmny} \tag{55}$$

$$H_y^{IIyc} = \frac{-j\omega}{k_0^2} \sum_{r=1}^{R} \sum_{p,q} A_{rpq} \sum_{m,n}^{\infty} \frac{-\varepsilon_0}{k_I} \frac{\varepsilon_{0m}\varepsilon_{0n}}{ab \sin(k_I c)} \left(k_0^2 - \left(\frac{n\pi}{b}\right)^2\right) \cos\left(\frac{m\pi x}{a}\right) \sin\left(\frac{n\pi y}{b}\right)$$
$$\cos(k_I z) I_{rpqmny} \tag{56}$$

$$H_z^{IIyc} = \frac{-j\omega}{k_0^2} \sum_{r=1}^{R} \sum_{p,q} A_{rpq} \sum_{m,n}^{\infty} \frac{-\varepsilon_0}{k_I} \frac{\varepsilon_{0m}\varepsilon_{0n}}{ab \sin(k_I c)} \frac{n\pi}{b} (-k_I) \cos\left(\frac{m\pi x}{a}\right) \cos\left(\frac{n\pi y}{b}\right)$$
$$\sin(k_I z) I_{rpqmny} \tag{57}$$

For a unique solution the electromagnetic fields in various regions must satisfy continuity conditions over their common surfaces. The tangential electric fields over the apertures are continuous. The tangential magnetic fields over the apertures must also be continuous, thus yielding coupled

integral equations with the magnetic currents as unknown variables. The coupled integral equation in conjunction with the method of moments can be solved for the amplitudes of magnetic currents.

2.3 Derivation of Integral Equation

The total tangential magnetic fields inside the cavity from apertures on both sides are written as

$$H_x^{II} = (H_x^{IIx0} + H_x^{IIy0} + H_x^{IIxc} + H_x^{IIyc})$$

$$H_y^{II} = (H_y^{IIx0} + H_y^{IIy0} + H_y^{IIxc} + H_y^{IIyc})$$

Using continuity of tangential magnetic fields across the apertures in the $z = 0$ plane yields

$$H_{xi}\Big|_{z=0} + H_x^I\Big|_{z=0} = (H_x^{IIx0} + H_x^{IIy0} + H_x^{IIxc} + H_x^{IIyc})\Big|_{z=0} \tag{58}$$

$$H_{yi}\Big|_{z=0} + H_y^I\Big|_{z=0} = (H_y^{IIx0} + H_y^{IIy0} + H_y^{IIxc} + H_y^{IIyc})\Big|_{z=0} \tag{59}$$

And matching the tangential magnetic fields across the apertures in $z = c$ plane yields

$$(H_x^{IIx0} + H_x^{IIy0} + H_x^{IIxc} + H_x^{IIyc})\Big|_{z=c} = H_x^{III}\Big|_{z=c} \tag{60}$$

$$(H_y^{IIx0} + H_y^{IIy0} + H_y^{IIxc} + H_y^{IIyc})\Big|_{z=c} = H_y^{III}\Big|_{z=c} \tag{61}$$

In deriving equations (58)-(61) it is assumed that the cavity is excited by a plane wave incident from $z = -\infty$.

2.3.1 Integral Equation for Apertures on $z = 0$ Plane

Using the field expressions derived in the earlier sections, equation (58) can be written as

$$H_{xi} + \sum_{r=1}^{R} \sum_{pq} \frac{\omega \varepsilon_0 U_{rpq}}{4\pi^2 k_0^2} \int_{-\infty}^{\infty} \int_{-\infty}^{\infty} \Psi_{rpqx} \frac{(k_0^2 - k_x^2)}{k_I} e^{jk_x x + jk_y y} dk_x dk_y$$

$$+\sum_{r=1}^{R}\sum_{pq}\frac{-\omega\varepsilon_0 V_{rpq}}{4\pi^2 k_0^2}\int_{-\infty}^{\infty}\int_{-\infty}^{\infty}\phi_{rpqy}\frac{(-k_x k_y)}{k_I}e^{jk_x x+jk_y y}dk_x dk_y$$

$$=\frac{-j\omega}{k_0^2}\sum_{r=1}^{R}\sum_{p,q}U_{rpq}\sum_{m,n}^{\infty}\frac{-\varepsilon_0}{k_I}\frac{\varepsilon_{0m}\varepsilon_{0n}}{ab\sin(k_I c)}\left(k_0^2-\left(\frac{m\pi}{a}\right)^2\right)\sin\left(\frac{m\pi x}{a}\right)\cos\left(\frac{n\pi y}{b}\right)$$

$$\cos(k_I c)I_{rpqmnx}$$

$$\frac{-j\omega}{k_0^2}\sum_{r=1}^{R}\sum_{p,q}-V_{rpq}\sum_{m,n}^{\infty}\frac{-\varepsilon_0}{k_I}\frac{\varepsilon_{0m}\varepsilon_{0n}}{ab\sin(k_I c)}\left(-\frac{m\pi}{a}\right)\frac{n\pi}{b}\sin\left(\frac{m\pi x}{a}\right)\cos\left(\frac{n\pi y}{b}\right)$$

$$\cos(k_I c)I_{rpqmny}$$

$$\frac{-j\omega}{k_0^2}\sum_{r=1}^{R}\sum_{p,q}(-B_{rqp})\sum_{m,n}^{\infty}\frac{-\varepsilon_0}{k_I}\left(\frac{\varepsilon_{0m}\varepsilon_{0n}}{ab\sin(k_I c)}I_{rpqmnx}\right)\left(k_0^2-\left(\frac{m\pi}{a}\right)^2\right)\sin\left(\frac{m\pi x}{a}\right)\cos\left(\frac{n\pi y}{b}\right)$$

$$\frac{-j\omega}{k_0^2}\sum_{r=1}^{R}\sum_{p,q}A_{rpq}\sum_{m,n}^{\infty}\frac{-\varepsilon_0}{k_I}\left(\frac{\varepsilon_{0m}\varepsilon_{0n}}{ab\sin(k_I c)}I_{rpqmny}\right)\left(-\frac{m\pi}{a}\right)\frac{n\pi}{b}\sin\left(\frac{m\pi x}{a}\right)\cos\left(\frac{n\pi y}{b}\right) \quad (62)$$

Now selecting $\Psi_{r'p'q'x}$ as a testing function and use of Galerkin's method reduces the above equation to

$$I_{r'p'q'xi}+\sum_{r=1}^{R}\sum_{pq}\frac{\omega\varepsilon_0 U_{rpq}}{4\pi^2 k_0^2}\int_{-\infty}^{\infty}\int_{-\infty}^{\infty}\Psi_{rpqx}\Psi^{*}_{r'p'q'x}\frac{(k_0^2-k_x^2)}{k_I}dk_x dk_y$$

$$+\sum_{r=1}^{R}\sum_{pq}\frac{-\omega\varepsilon_0 V_{rpq}}{4\pi^2 k_0^2}\int_{-\infty}^{\infty}\int_{-\infty}^{\infty}(\phi_{rpqy}\Psi^{*}_{r'p'q'x})\frac{(-k_x k_y)}{k_I}dk_x dk_y$$

$$=\frac{-j\omega}{k_0^2}\sum_{r=1}^{R}\sum_{p,q}U_{rpq}\sum_{m,n}^{\infty}\frac{-\varepsilon_0}{k_I}\frac{\varepsilon_{0m}\varepsilon_{0n}}{ab\sin(k_I c)}\left(k_0^2-\left(\frac{m\pi}{a}\right)^2\right)\cos(k_I c)I_{rpqmnx}I_{r'p'q'mnx}$$

$$\frac{-j\omega}{k_0^2}\sum_{r=1}^{R}\sum_{p,q}-V_{rpq}\sum_{m,n}^{\infty}\frac{-\varepsilon_0}{k_I}\frac{\varepsilon_{0m}\varepsilon_{0n}}{ab\sin(k_I c)}\left(-\frac{m\pi}{a}\right)\frac{n\pi}{b}\cos(k_I c)I_{rpqmny}I_{r'p'q'mnx}$$

$$\frac{-j\omega}{k_0^2}\sum_{r=1}^{R}\sum_{p,q}(-B_{rqp})\sum_{m,n}^{\infty}\frac{-\varepsilon_0}{k_I}\left(\frac{\varepsilon_{0m}\varepsilon_{0n}}{ab\sin(k_I c)}I_{rpqmnx}I_{r'p'q'mnx}\right)\left(k_0^2-\left(\frac{m\pi}{a}\right)^2\right)$$

$$\frac{-j\omega}{k_0^2}\sum_{r=1}^{R}\sum_{p,q}A_{rpq}\sum_{m,n}^{\infty}\frac{-\varepsilon_0}{k_I}\left(\frac{\varepsilon_{0m}\varepsilon_{0n}}{ab\sin(k_I c)}I_{rpqmny}I_{r'p'q'mnx}\right)\left(-\frac{m\pi}{a}\right)\frac{n\pi}{b} \quad (63)$$

Rearranging the terms in (63) we get

$$I_{r'p'q'xi} = \sum_{r=1}^{R}\sum_{pq}\left(U_{rpq}Y^{x1x1}_{rpqr'p'q'} + V_{rpq}Y^{x1y1}_{rpqr'p'q'} + A_{rpq}Y^{x1y2}_{rpqr'p'q'} + B_{rqp}Y^{x1x2}_{rpqr'p'q'}\right) \quad (64)$$

where

$$Y^{x1x1}_{rpqr'p'q'} = \frac{-j\omega}{k_0^2}\sum_{m,n}^{\infty}\frac{-\varepsilon_0}{k_I}\frac{\varepsilon_{0m}\varepsilon_{0n}}{ab\sin(k_I c)}\left(k_0^2-\left(\frac{m\pi}{a}\right)^2\right)\cos(k_I c)I_{rpqmnx}I_{r'p'q'mnx}$$

$$-\frac{\omega\varepsilon_0}{4\pi^2 k_0^2}\int_{-\infty}^{\infty}\int_{-\infty}^{\infty}\Psi_{rpqx}\Psi^{*}_{r'p'q'x}\frac{(k_0^2-k_x^2)}{k_z}dk_x dk_y \quad (65)$$

$$Y^{x1y1}_{rpqr'p'q'} = \frac{j\omega}{k_0^2}\sum_{m,n}^{\infty}\frac{-\varepsilon_0}{k_I}\frac{\varepsilon_{0m}\varepsilon_{0n}}{ab\sin(k_I c)}\left(-\frac{m\pi}{a}\right)\frac{n\pi}{b}\cos(k_I c)I_{rpqmny}I_{r'p'q'mnx}$$

$$+\frac{\omega\varepsilon_0}{4\pi^2 k_0^2}\int_{-\infty}^{\infty}\int_{-\infty}^{\infty}(\phi_{rpqy}\Psi^{*}_{r'p'q'x})\frac{(-k_x k_y)}{k_z}dk_x dk_y \quad (66)$$

$$Y^{x1x2}_{rpqr'p'q'} = \frac{j\omega}{k_0^2}\sum_{m,n}^{\infty}\frac{-\varepsilon_0}{k_I}\left(\frac{\varepsilon_{0m}\varepsilon_{0n}}{ab\sin(k_I c)}I_{rpqmnx}I_{r'p'q'mnx}\right)\left(k_0^2-\left(\frac{m\pi}{a}\right)^2\right) \quad (67)$$

$$Y^{x1y2}_{rpqr'p'q'} = \frac{-j\omega}{k_0^2}\sum_{m,n}^{\infty}\frac{-\varepsilon_0}{k_I}\left(\frac{\varepsilon_{0m}\varepsilon_{0n}}{ab\sin(k_I c)}I_{rpqmny}I_{r'p'q'mnx}\right)\left(-\frac{m\pi}{a}\right)\frac{n\pi}{b} \quad (68)$$

$$I_{r'p'q'xi} = \int_{r'p'q'}\int H_{xi}\Psi_{r'p'q'x}dxdy \quad (69)$$

Using expression (59) we get

$$H_{yi} + \sum_{r=1}^{R}\sum_{pq}\frac{-\omega\varepsilon_0 V_{rpq}}{4\pi^2 k_0^2}\int_{-\infty}^{\infty}\int_{-\infty}^{\infty}\phi_{rpqy}\frac{(k_0^2-k_y^2)}{k_z}e^{jk_x x + jk_y y}dk_x dk_y$$

$$+\sum_{r=1}^{R}\sum_{pq}\frac{\omega\varepsilon_0 U_{rpq}}{4\pi^2 k_0^2}\int_{-\infty}^{\infty}\int_{-\infty}^{\infty}\Psi_{rpqx}\frac{(-k_x k_y)}{k_z}e^{jk_x x + jk_y y}dk_x dk_y$$

$$= \frac{-j\omega}{k_0^2}\sum_{r=1}^{R}\sum_{p,q}U_{rpq}\sum_{m,n}^{\infty}\frac{-\varepsilon_0}{k_I}\frac{\varepsilon_{0m}\varepsilon_{0n}}{ab\sin(k_I c)}\frac{m\pi}{a}\left(-\frac{n\pi}{b}\right)\cos\left(\frac{m\pi x}{a}\right)\sin\left(\frac{n\pi y}{b}\right)$$

$$\cos(k_I c)I_{rpqmnx}$$

$$\frac{-j\omega}{k_0^2}\sum_{r=1}^{R}\sum_{p,q}-V_{rpq}\sum_{m,n}^{\infty}\frac{-\varepsilon_0}{k_I}\frac{\varepsilon_{0m}\varepsilon_{0n}}{ab\sin(k_I c)}\left(k_0^2-\left(\frac{n\pi}{b}\right)^2\right)\cos\left(\frac{m\pi x}{a}\right)\sin\left(\frac{n\pi y}{b}\right)$$

$$\cos(k_I c)I_{rpqmny}$$

$$\frac{-j\omega}{k_0^2}\sum_{r=1}^{R}\sum_{p,q}(-B_{rqp})\sum_{m,n}^{\infty}\frac{-\varepsilon_0}{k_I}\left(\frac{\varepsilon_{0m}\varepsilon_{0n}}{ab\sin(k_I c)}I_{rpqmnx}\right)\frac{m\pi}{a}\left(-\frac{n\pi}{b}\right)\cos\left(\frac{m\pi x}{a}\right)\sin\left(\frac{n\pi y}{b}\right)$$

$$\frac{-j\omega}{k_0^2}\sum_{r=1}^{R}\sum_{p,q}A_{rpq}\sum_{m,n}^{\infty}\frac{-\varepsilon_0}{k_I}\left(\frac{\varepsilon_{0m}\varepsilon_{0n}}{ab\sin(k_I c)}I_{rpqmny}\right)\left(k_0^2-\left(\frac{n\pi}{b}\right)^2\right)\cos\left(\frac{m\pi x}{a}\right)\sin\left(\frac{n\pi y}{b}\right) \tag{70}$$

Now selecting $-\Phi_{r'p'q'y}$ as a testing function and use of Galerkin's method yields

$$I_{r'p'q'yi} = \sum_{r=1}^{R}\sum_{pq}\frac{-\omega\varepsilon_0 V_{rpq}}{4\pi^2 k_0^2}\int_{-\infty}^{\infty}\int_{-\infty}^{\infty}\phi_{rpqy}\phi^{*}_{r'p'q'y}\frac{(k_0^2-k_y^2)}{k_z}dk_x dk_y$$

$$+\sum_{r=1}^{R}\sum_{pq}\frac{\omega\varepsilon_0 U_{rpq}}{4\pi^2 k_0^2}\int_{-\infty}^{\infty}\int_{-\infty}^{\infty}(\psi_{rpqx}\phi^{*}_{r'p'q'y})\frac{(-k_x k_y)}{k_z}dk_x dk_y$$

$$+\frac{j\omega}{k_0^2}\sum_{r=1}^{R}\sum_{p,q}U_{rpq}\sum_{m,n}^{\infty}\frac{-\varepsilon_0}{k_I}\frac{\varepsilon_{0m}\varepsilon_{0n}}{ab\sin(k_I c)}\frac{m\pi}{a}\left(-\frac{n\pi}{b}\right)\cos(k_I c)I_{rpqmnx}I_{r'pq'mny}$$

$$+\frac{j\omega}{k_0^2}\sum_{r=1}^{R}\sum_{p,q}-V_{rpq}\sum_{m,n}^{\infty}\frac{-\varepsilon_0}{k_I}\frac{\varepsilon_{0m}\varepsilon_{0n}}{ab\sin(k_I c)}\left(k_0^2-\left(\frac{n\pi}{b}\right)^2\right)\cos(k_I c)I_{rpqmny}I_{r'pq'mny}$$

$$+\frac{j\omega}{k_0^2}\sum_{r=1}^{R}\sum_{p,q}(-B_{rqp})\sum_{m,n}^{\infty}\frac{-\varepsilon_0}{k_I}\left(\frac{\varepsilon_{0m}\varepsilon_{0n}}{ab\sin(k_I c)}I_{rpqmnx}I_{r'pq'mny}\right)\frac{m\pi}{a}\left(-\frac{n\pi}{b}\right)$$

$$+\frac{j\omega}{k_0^2}\sum_{r=1}^{R}\sum_{p,q}A_{rpq}\sum_{m,n}^{\infty}\frac{-\varepsilon_0}{k_I}\left(\frac{\varepsilon_{0m}\varepsilon_{0n}}{ab\sin(k_I c)}I_{rpqmny}I_{r'pq'mny}\right)\left(k_0^2-\left(\frac{n\pi}{b}\right)^2\right) \tag{71}$$

Rearranging the terms in (71) we get

$$I_{r'p'q'yi} = \sum_{r=1}^{R}\sum_{pq}\left(U_{rpq}Y^{y1x1}_{rpqr'p'q'} + V_{rpq}Y^{y1y1}_{rpqr'p'q'} + A_{rpq}Y^{y1y2}_{rpqr'p'q'} + B_{rqp}Y^{y1x2}_{rpqr'p'q'}\right) \tag{72}$$

where

$$Y^{y1x1}_{rpqr'p'q'} = \frac{\omega\varepsilon_0}{4\pi^2 k_0^2}\int_{-\infty}^{\infty}\int_{-\infty}^{\infty}(\psi_{rpqx}\phi^{*}_{r'p'q'y})\frac{(-k_x k_y)}{k_z}dk_x dk_y$$

$$+\frac{j\omega}{k_0^2}\sum_{m,\,n}^{\infty}\frac{-\varepsilon_0}{k_I}\frac{\varepsilon_{0m}\varepsilon_{0n}}{ab\sin(k_I c)}\frac{m\pi}{a}\left(-\frac{n\pi}{b}\right)\cos(k_I c)I_{rpqmnx}I_{r'pq'mny} \tag{73}$$

$$Y^{y1y1}_{rpqr'p'q'} = \frac{-\omega\varepsilon_0}{4\pi^2 k_0^2}\int_{-\infty}^{\infty}\int_{-\infty}^{\infty}\phi_{rpqy}\phi^{*}_{r'p'q'y}\frac{(k_0^2-k_y^2)}{k_z}dk_x dk_y$$

$$\frac{-j\omega}{k_0^2}\sum_{m,\,n}^{\infty}\frac{-\varepsilon_0}{k_I}\frac{\varepsilon_{0m}\varepsilon_{0n}}{ab\sin(k_I c)}\left(k_0^2-\left(\frac{n\pi}{b}\right)^2\right)\cos(k_I c)I_{rpqmny}I_{r'pq'mny} \tag{74}$$

$$Y^{y1x2}_{rpqr'p'q'} = \frac{-j\omega}{k_0^2}\sum_{m,\,n}^{\infty}\frac{-\varepsilon_0}{k_I}\left(\frac{\varepsilon_{0m}\varepsilon_{0n}}{ab\sin(k_I c)}I_{rpqmnx}I_{r'pq'mny}\right)\frac{m\pi}{a}\left(-\frac{n\pi}{b}\right) \tag{75}$$

$$Y^{y1y2}_{rpqr'p'q'} = +\frac{j\omega}{k_0^2}\sum_{m,\,n}^{\infty}\frac{-\varepsilon_0}{k_I}\left(\frac{\varepsilon_{0m}\varepsilon_{0n}}{ab\sin(k_I c)}I_{rpqmny}I_{r'pq'mny}\right)\left(k_0^2-\left(\frac{n\pi}{b}\right)^2\right) \tag{76}$$

$$I_{r'p'q'yi} = -\int_{r'p'q'}\int H_{yi}\Phi_{r'p'q'x}dxdy \tag{77}$$

2.3.2 Integral Equations for Apertures on $z = c$ Plane

Using (60), we get

$$\frac{-j\omega}{k_0^2}\sum_{r\,=\,1}^{R}\sum_{p,\,q}U_{rpq}\sum_{m,\,n}^{\infty}\frac{-\varepsilon_0}{k_I}\left(\frac{\varepsilon_{0m}\varepsilon_{0n}}{ab\sin(k_I c)}I_{rpqmnx}\right)\left(k_0^2-\left(\frac{m\pi}{a}\right)^2\right)\sin\left(\frac{m\pi x}{a}\right)\cos\left(\frac{n\pi y}{b}\right)$$

$$\frac{-j\omega}{k_0^2}\sum_{r\,=\,1}^{R}\sum_{p,\,q}-V_{rpq}\sum_{m,\,n}^{\infty}\frac{-\varepsilon_0}{k_I}\left(\frac{\varepsilon_{0m}\varepsilon_{0n}}{ab\sin(k_I c)}I_{rpqmny}\right)\left(-\frac{m\pi}{a}\right)\frac{n\pi}{b}\sin\left(\frac{m\pi x}{a}\right)\cos\left(\frac{n\pi y}{b}\right)$$

$$\frac{-j\omega}{k_0^2}\sum_{r\,=\,1}^{R}\sum_{p,\,q}(-B_{rqp})\sum_{m,\,n}^{\infty}\frac{-\varepsilon_0}{k_I}\frac{\varepsilon_{0m}\varepsilon_{0n}}{ab\sin(k_I c)}\left(k_0^2-\left(\frac{m\pi}{a}\right)^2\right)\sin\left(\frac{m\pi x}{a}\right)\cos\left(\frac{n\pi y}{b}\right)$$

$$\cos(k_I c) I_{rpqmnx}$$

$$\frac{-j\omega}{k_0^2}\sum_{r=1}^{R}\sum_{p,q} A_{rpq}\sum_{m,n}^{\infty}\frac{-\varepsilon_0}{k_I}\frac{\varepsilon_{0m}\varepsilon_{0n}}{ab\sin(k_I c)}\left(-\frac{m\pi}{a}\right)\frac{n\pi}{b}\sin\left(\frac{m\pi x}{a}\right)\cos\left(\frac{n\pi y}{b}\right)$$

$$\cos(k_I c) I_{rpqmny}$$

$$= \sum_{r=1}^{R}\sum_{pq}\frac{-\omega\varepsilon_0 B_{rpq}}{4\pi^2 k_0^2}\int_{-\infty}^{\infty}\int_{-\infty}^{\infty}\psi_{rpqx}\frac{(k_0^2-k_x^2)}{k_I}e^{jk_x x + jk_y y}dk_x dk_y$$

$$+\sum_{r=1}^{R}\sum_{pq}\frac{\omega\varepsilon_0 A_{rpq}}{4\pi^2 k_0^2}\int_{-\infty}^{\infty}\int_{-\infty}^{\infty}\phi_{rpqy}\frac{(-k_x k_y)}{k_I}e^{jk_x x + jk_y y}dk_x dk_y \qquad (78)$$

Now selecting testing function $-\Psi_{r'p'q'x}$ and use of Galerkin's method yields

$$0 = \frac{-j\omega}{k_0^2}\sum_{r=1}^{R}\sum_{p,q} U_{rpq}\sum_{m,n}^{\infty}\frac{-\varepsilon_0}{k_I}\frac{\varepsilon_{0m}\varepsilon_{0n}}{ab\sin(k_I c)} I_{rpqmnx} I_{r'p'q'mnx}\left(k_0^2-\left(\frac{m\pi}{a}\right)^2\right)$$

$$+\frac{j\omega}{k_0^2}\sum_{r=1}^{R}\sum_{p,q} -V_{rpq}\sum_{m,n}^{\infty}\frac{-\varepsilon_0}{k_I}\frac{\varepsilon_{0m}\varepsilon_{0n}}{ab\sin(k_I c)} I_{rpqmny} I_{r'p'q'mnx}\left(-\frac{m\pi}{a}\right)\frac{n\pi}{b}$$

$$\frac{-j\omega}{k_0^2}\sum_{r=1}^{R}\sum_{p,q}(-B_{rqp})\sum_{m,n}^{\infty}\frac{-\varepsilon_0}{k_I}\frac{\varepsilon_{0m}\varepsilon_{0n}}{ab\sin(k_I c)}\left(k_0^2-\left(\frac{m\pi}{a}\right)^2\right)\cos(k_I c) I_{rpqmnx} I_{r'p'q'mnx}$$

$$\frac{-j\omega}{k_0^2}\sum_{r=1}^{R}\sum_{p,q} A_{rpq}\sum_{m,n}^{\infty}\frac{-\varepsilon_0}{k_I}\frac{\varepsilon_{0m}\varepsilon_{0n}}{ab\sin(k_I c)}\left(-\frac{m\pi}{a}\right)\frac{n\pi}{b}\cos(k_I c) I_{rpqmny} I_{r'p'q'mnx}$$

$$+\sum_{r=1}^{R}\sum_{pq}\frac{\omega\varepsilon_0 B_{rpq}}{4\pi^2 k_0^2}\int_{-\infty}^{\infty}\int_{-\infty}^{\infty}\psi_{rpqx}\psi^{*}_{r'p'q'x}\frac{(k_0^2-k_x^2)}{k_z}dk_x dk_y$$

$$-\sum_{r=1}^{R}\sum_{pq}\frac{\omega\varepsilon_0 A_{rpq}}{4\pi^2 k_0^2}\int_{-\infty}^{\infty}\int_{-\infty}^{\infty}\phi_{rpqy}\psi^{*}_{r'p'q'x}\frac{(-k_x k_y)}{k_z}dk_x dk_y \qquad (79)$$

Rearranging the terms in (79) we get

$$0 = \sum_{r=1}^{R}\sum_{pq}\left(U_{rpq}Y^{x2x1}_{rpqr'p'q'} + V_{rpq}Y^{x2y1}_{rpqr'p'q'} + A_{rpq}Y^{x2y2}_{rpqr'p'q'} + B_{rqp}Y^{x2x2}_{rpqr'p'q'}\right) \qquad (80)$$

where

$$Y^{x2x1}_{rpqr'p'q'} = \frac{-j\omega}{k_0^2}\sum_{m,\,n}^{\infty}\frac{-\varepsilon_0}{k_I}\frac{\varepsilon_{0m}\varepsilon_{0n}}{ab\sin(k_I c)}I_{rpqmnx}I_{r'p'q'mnx}\left(k_0^2-\left(\frac{m\pi}{a}\right)^2\right) \tag{81}$$

$$Y^{x2y1}_{rpqr'p'q'} = -\frac{j\omega}{k_0^2}\sum_{m,\,n}^{\infty}\frac{-\varepsilon_0}{k_I}\frac{\varepsilon_{0m}\varepsilon_{0n}}{ab\sin(k_I c)}I_{rpqmny}I_{r'p'q'mnx}\left(-\frac{m\pi}{a}\right)\frac{n\pi}{b} \tag{82}$$

$$Y^{x2x2}_{rpqr'p'q'} = \frac{j\omega}{k_0^2}\sum_{m,\,n}^{\infty}\frac{-\varepsilon_0}{k_I}\frac{\varepsilon_{0m}\varepsilon_{0n}}{ab\sin(k_I c)}\left(k_0^2-\left(\frac{m\pi}{a}\right)^2\right)\cos(k_I c)I_{rpqmnx}I_{r'p'q'mnx}$$

$$+\frac{\omega\varepsilon_0}{4\pi^2 k_0^2}\int_{-\infty}^{\infty}\int_{-\infty}^{\infty}\psi_{rpqx}\psi^{*}_{r'p'q'x}\frac{(k_0^2-k_x^2)}{k_z}dk_x dk_y \tag{83}$$

$$Y^{x2y2}_{rpqr'p'q'} = \frac{-j\omega}{k_0^2}\sum_{m,\,n}^{\infty}\frac{-\varepsilon_0}{k_I}\frac{\varepsilon_{0m}\varepsilon_{0n}}{ab\sin(k_I c)}\left(-\frac{m\pi}{a}\right)\frac{n\pi}{b}\cos(k_I c)I_{rpqmny}I_{r'p'q'mnx}$$

$$-\frac{\omega\varepsilon_0}{4\pi^2 k_0^2}\int_{-\infty}^{\infty}\int_{-\infty}^{\infty}\phi_{rpqy}\psi^{*}_{r'p'q'x}\frac{(-k_x k_y)}{k_z}dk_x dk_y \tag{84}$$

From (61) we get

$$\frac{-j\omega}{k_0^2}\sum_{r\,=\,1}^{R}\sum_{p,\,q}U_{rpq}\sum_{m,\,n}^{\infty}\frac{-\varepsilon_0}{k_I}\left(\frac{\varepsilon_{0m}\varepsilon_{0n}}{ab\sin(k_I c)}I_{rpqmnx}\right)\frac{m\pi}{a}\left(-\frac{n\pi}{b}\right)\cos\left(\frac{m\pi x}{a}\right)\sin\left(\frac{n\pi y}{b}\right)$$

$$\frac{-j\omega}{k_0^2}\sum_{r\,=\,1}^{R}\sum_{p,\,q}-V_{rpq}\sum_{m,\,n}^{\infty}\frac{-\varepsilon_0}{k_I}\left(\frac{\varepsilon_{0m}\varepsilon_{0n}}{ab\sin(k_I c)}I_{rpqmny}\right)\left(k_0^2-\left(\frac{n\pi}{b}\right)^2\right)\cos\left(\frac{m\pi x}{a}\right)\sin\left(\frac{n\pi y}{b}\right)$$

$$\frac{-j\omega}{k_0^2}\sum_{r\,=\,1}^{R}\sum_{p,\,q}(-B_{rqp})\sum_{m,\,n}^{\infty}\frac{-\varepsilon_0}{k_I}\frac{\varepsilon_{0m}\varepsilon_{0n}}{ab\sin(k_I c)}\frac{m\pi}{a}\left(-\frac{n\pi}{b}\right)\cos\left(\frac{m\pi x}{a}\right)\sin\left(\frac{n\pi y}{b}\right)$$

$$\cos(k_I c) I_{rpqmnx}$$

$$\frac{-j\omega}{k_0^2}\sum_{r=1}^{R}\sum_{p,q} A_{rpq}\sum_{m,n}^{\infty}\frac{-\varepsilon_0}{k_I}\frac{\varepsilon_{0m}\varepsilon_{0n}}{ab\sin(k_I c)}\left(k_0^2-\left(\frac{n\pi}{b}\right)^2\right)\cos\left(\frac{m\pi x}{a}\right)\sin\left(\frac{n\pi y}{b}\right)$$

$$\cos(k_I c) I_{rpqmny}$$

$$= \sum_{r=1}^{R}\sum_{pq}\frac{\omega\varepsilon_0 A_{rpq}}{4\pi^2 k_0^2}\int_{-\infty}^{\infty}\int_{-\infty}^{\infty}\phi_{rpqy}\frac{(k_0^2-k_y^2)}{k_z}e^{jk_x x + jk_y y}dk_x dk_y$$

$$+ \sum_{r=1}^{R}\sum_{pq}\frac{-\omega\varepsilon_0 B_{rpq}}{4\pi^2 k_0^2}\int_{-\infty}^{\infty}\int_{-\infty}^{\infty}\psi_{pqx}\frac{(-k_x k_y)}{k_z}e^{jk_x x + jk_y y}dk_x dk_y \qquad (85)$$

Now selecting $\Phi_{r'p'q'y}$ as a testing function and use of Galerkin's method yields

$$0 = \frac{j\omega}{k_0^2}\sum_{r=1}^{R}\sum_{p,q} U_{rpq}\sum_{m,n}^{\infty}\frac{-\varepsilon_0}{k_I}\frac{\varepsilon_{0m}\varepsilon_{0n}}{ab\sin(k_I c)} I_{rpqmnx} I_{r'p'q'mny}\frac{m\pi}{a}\left(-\frac{n\pi}{b}\right)$$

$$+ \frac{j\omega}{k_0^2}\sum_{r=1}^{R}\sum_{p,q} -V_{rpq}\sum_{m,n}^{\infty}\frac{-\varepsilon_0}{k_I}\frac{\varepsilon_{0m}\varepsilon_{0n}}{ab\sin(k_I c)} I_{rpqmny} I_{r'p'q'mny}\left(k_0^2-\left(\frac{n\pi}{b}\right)^2\right)$$

$$+ \frac{j\omega}{k_0^2}\sum_{r=1}^{R}\sum_{p,q} (-B_{rqp})\sum_{m,n}^{\infty}\frac{-\varepsilon_0}{k_I}\frac{\varepsilon_{0m}\varepsilon_{0n}}{ab\sin(k_I c)}\frac{m\pi}{a}\left(-\frac{n\pi}{b}\right)\cos(k_I c) I_{rpqmnx} I_{r'p'q'mny}$$

$$+ \sum_{r=1}^{R}\sum_{pq}\frac{-\omega\varepsilon_0 B_{rpq}}{4\pi^2 k_0^2}\int_{-\infty}^{\infty}\int_{-\infty}^{\infty}\psi_{pqx}\phi_{r'p'q'y}\frac{(-k_x k_y)}{k_z}dk_x dk_y$$

$$+ \frac{j\omega}{k_0^2}\sum_{r=1}^{R}\sum_{p,q} A_{rpq}\sum_{m,n}^{\infty}\frac{-\varepsilon_0}{k_I}\frac{\varepsilon_{0m}\varepsilon_{0n}}{ab\sin(k_I c)}\left(k_0^2-\left(\frac{n\pi}{b}\right)^2\right)\cos(k_I c) I_{rpqmny} I_{r'p'q'mny}$$

$$+ \sum_{r=1}^{R}\sum_{pq}\frac{\omega\varepsilon_0 A_{rpq}}{4\pi^2 k_0^2}\int_{-\infty}^{\infty}\int_{-\infty}^{\infty}\phi_{rpqy}\phi_{r'p'q'y}\frac{(k_0^2-k_y^2)}{k_z}dk_x dk_y \qquad (86)$$

Rearranging the terms in (84) we get

$$0 = \sum_{r=1}^{R}\sum_{pq}\left(U_{rpq}Y^{y2x1}_{rpqr'p'q'} + V_{rpq}Y^{y2y1}_{rpqr'p'q'} + A_{rpq}Y^{y2y2}_{rpqr'p'q'} + B_{rqp}Y^{y2x2}_{rpqr'p'q'}\right) \qquad (87)$$

where

$$Y^{y2x1}_{rpqr'p'q'} = \frac{j\omega}{k_0^2}\sum_{m,\,n}^{\infty}\frac{-\varepsilon_0}{k_I}\frac{\varepsilon_{0m}\varepsilon_{0n}}{ab\sin(k_I c)}I_{rpqmnx}I_{r'p'q'mny}\frac{m\pi}{a}\left(-\frac{n\pi}{b}\right) \tag{88}$$

$$Y^{y2y1}_{rpqr'p'q'} = \frac{-j\omega}{k_0^2}\sum_{m,\,n}^{\infty}\frac{-\varepsilon_0}{k_I}\frac{\varepsilon_{0m}\varepsilon_{0n}}{ab\sin(k_I c)}I_{rpqmny}I_{r'p'q'mny}\left(k_0^2-\left(\frac{n\pi}{b}\right)^2\right) \tag{89}$$

$$Y^{y2x2}_{rpqr'p'q'} = \frac{-j\omega}{k_0^2}\sum_{m,\,n}^{\infty}\frac{-\varepsilon_0}{k_I}\frac{\varepsilon_{0m}\varepsilon_{0n}}{ab\sin(k_I c)}\frac{m\pi}{a}\left(-\frac{n\pi}{b}\right)\cos(k_I c)I_{rpqmnx}I_{r'p'q'mny}$$

$$+\frac{-\omega\varepsilon_0}{4\pi^2 k_0^2}\int_{-\infty}^{\infty}\int_{-\infty}^{\infty}\psi_{pqx}\phi^{*}_{r'p'q'y}\frac{(-k_x k_y)}{k_z}dk_x dk_y \tag{90}$$

$$Y^{y2y2}_{rpqr'p'q'} = \frac{j\omega}{k_0^2}\sum_{m,\,n}^{\infty}\frac{-\varepsilon_0}{k_I}\frac{\varepsilon_{0m}\varepsilon_{0n}}{ab\sin(k_I c)}\left(k_0^2-\left(\frac{n\pi}{b}\right)^2\right)\cos(k_I c)I_{rpqmny}I_{r'p'q'mny}$$

$$+\frac{\omega\varepsilon_0}{4\pi^2 k_0^2}\int_{-\infty}^{\infty}\int_{-\infty}^{\infty}\phi_{rpqy}\phi^{*}_{r'p'q'y}\frac{(k_0^2-k_y^2)}{k_z}dk_x dk_y \tag{91}$$

Equations (64), (72), (80), and (87) can be written in a matrix form as

$$\begin{bmatrix} Y^{x1x1}_{rpqr'p'q'} & Y^{x1y1}_{rpqr'p'q'} & Y^{x1y2}_{rpqr'p'q'} & Y^{x1x2}_{rpqr'p'q'} \\ Y^{y1x1}_{rpqr'p'q'} & Y^{y1y1}_{rpqr'p'q'} & Y^{y1y2}_{rpqr'p'q'} & Y^{y1x2}_{rpqr'p'q'} \\ Y^{x2x1}_{rpqr'p'q'} & Y^{x2y1}_{rpqr'p'q'} & Y^{x2y2}_{rpqr'p'q'} & Y^{x2x2}_{rpqr'p'q'} \\ Y^{y2x1}_{rpqr'p'q'} & Y^{y2y1}_{rpqr'p'q'} & Y^{y2y2}_{rpqr'p'q'} & Y^{y2x2}_{rpqr'p'q'} \end{bmatrix}\begin{bmatrix} U_{rpq} \\ V_{rpq} \\ A_{rpq} \\ B_{rqp} \end{bmatrix} = \begin{bmatrix} I_{r'p'q'xi} \\ I_{r'p'q'yi} \\ 0 \\ 0 \end{bmatrix} \tag{92}$$

The matrix equation (92) can be numerically solved for the unknown amplitudes of equivalent magnetic currents induced on the apertures due to given incident field. From the knowledge of these amplitudes electromagnetic field inside as well as outside the cavity can be determined. The shielding effectiveness of the enclosure with rectangular apertures is then determined from the

EM fields using following expression [3]

$$E-Shielding(dB) = -20.\log\left(\frac{\left|\vec{E}_{int}\right|}{\left|\vec{E}_{ext}\right|}\right) \tag{93}$$

where $\vec{E}_{int}$ is the total electric field at a given point inside the enclosure and $\vec{E}_{ext}$ is the field at the same point in absence of the enclosure. The expressions for electric field components inside the cavity due external EM sources are given in Appendix IV.

3.0 Numerical Results & Discussions

3.1 Single Aperture Case

In this section we consider a variety of simple cases and compare the numerical results obtained using the present method with results published earlier [3] for validation of the computer code.

Consider a rectangular enclosure with single rectangular aperture on the $z = 0$ plane and illuminated by a plane wave at normal incidence polarized in the x-direction (as shown in Figure 3). The matrix equation (92) for this case reduces to

$$\begin{bmatrix} Y^{x1x1}_{rpqr'p'q'} & Y^{x1y1}_{rpqr'p'q'} \\ Y^{y1x1}_{rpqr'p'q'} & Y^{y1y1}_{rpqr'p'q'} \end{bmatrix} \begin{bmatrix} U_{rpq} \\ V_{rpq} \end{bmatrix} = \begin{bmatrix} I_{r'p'q'xi} \\ 0 \end{bmatrix} \tag{94}$$

For normal incidence

$$I_{r'p'q'xi} = \begin{cases} H_{xi} W_r \left(\dfrac{1-\cos(p'\pi)}{(p'\pi)/L_{r'}}\right), & for(q' = 0) \\ 0, & for(q' \neq 0) \end{cases}$$

Using the orthogonality of expansion functions it can be shown $Y^{x1y1}_{rpqr'p'q'} = Y^{y1x1}_{rpqr'p'q'} = 0$, hence equation (93) simplifies to

$$\left[Y^{x1x1}_{rpqr'p'q'}\right]\left[U_{rpq}\right] = \left[I_{r'p'q'xi}\right] \tag{95}$$

Furthermore, it has been found from numerical results that the expansion modes $p = 1, 3, 5, \ldots,$ and $q = 0$ are strongly excited. In equation (95) p' and q' are $p' = 1, 3, 5, \ldots$ and $q' = 0$

For a numerical solution of (94) we consider a rectangular cavity with $a = 30$ cms, $b = 12$ cms, and $c = 30$ cms with a rectangular aperture of size $(10x0.5)$ cms^2, located at $(15, 6, 0)$ cms, and illuminated by a plane wave at normal incidence. Assuming only $p = 1, q = 0$ expansion mode on the aperture and considering only dominant $m = 1, n = 0$ mode inside the cavity, electric field shielding obtained using expression (93) is plotted in Figure 3.1 along with the results from [3]. It is observed that the numerical data obtained using the present method agrees well with the earlier published results. Experimental data from [3] is also reproduced in Figure 3.1.

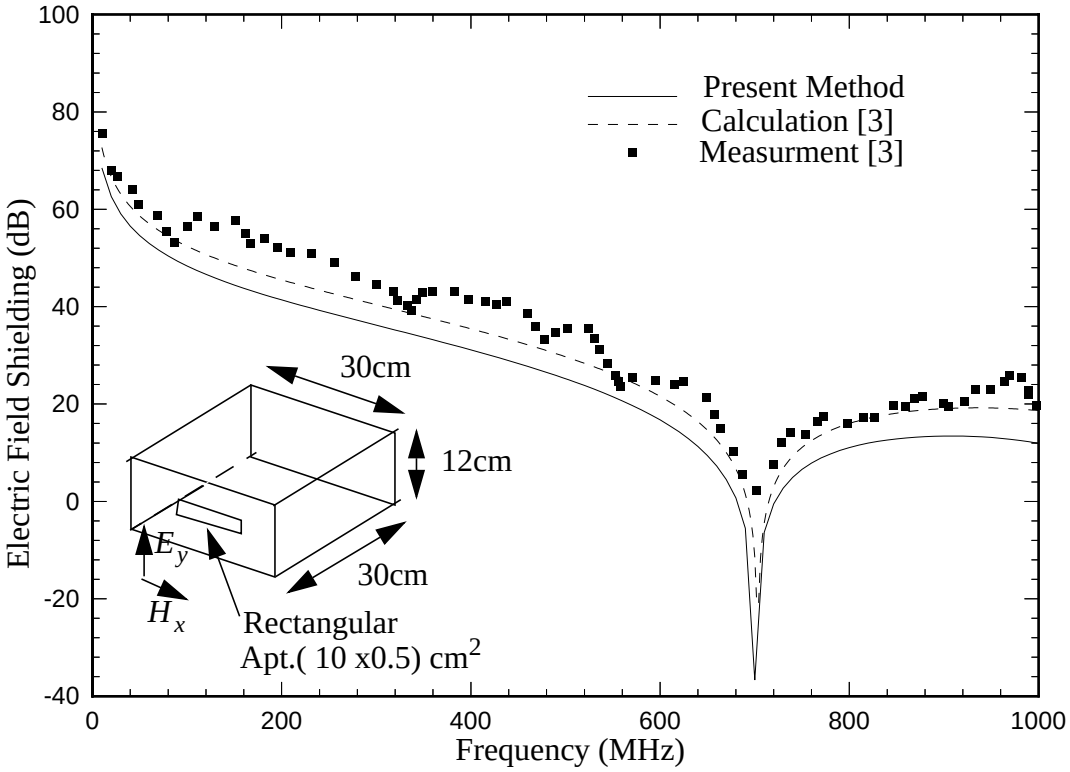

Figure 3.1 Electric field shielding at the center of 30 cm x 12 cm x 30 cm enclosure with 10 x 0.5 cm^2 aperture located at 15 x 6 cm in z=0 plane with dominant cavity mode considered.

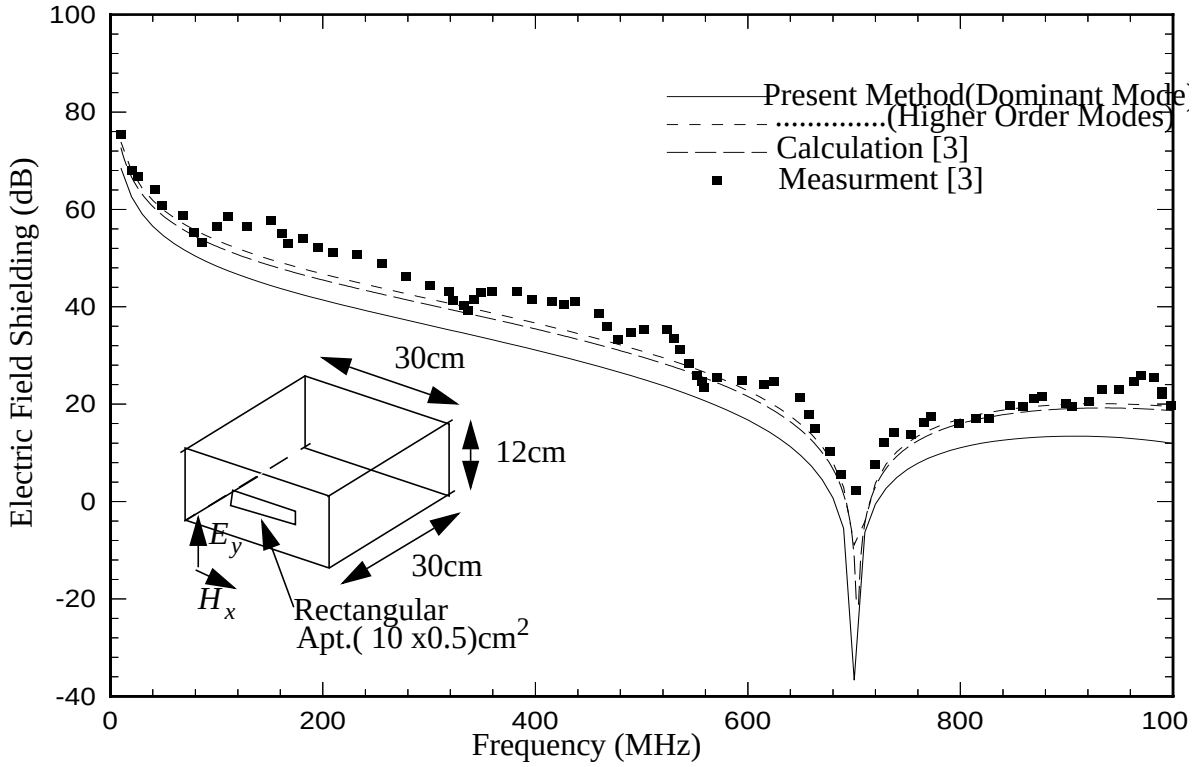

Figure 3.2 Electric field shielding at the center of 30 cm x 12 cm x 30 cm enclosure with 10 x 0.5 cm^2 aperture located at 15 x 6 cm in z=0 plane when higher order modes inside cavity and single mode on aperture were considered.

In order to study the effect of higher order modes, the electric field shielding is calculated using the present method with $p = 1, q = 0$ expansion mode and $p' = 1, q' = 0$ on the aperture and considering $m - max = 1200, n - max = 200$ modes including dominant mode inside the cavity. The electric field shielding obtained using the present method is plotted in Figure 3.2 along with the results from [3]. The numerical data in Figure 3.2 shows that consideration of higher order modes inside the cavity gives results closer to the measured values. Through numerical calculations, it was also noted that inclusion of higher order modes on the aperture did not alter the electric field shielding values shown in Figure 3.2.

To validate the present method for a wider aperture, the electric field shielding of a rectan-

gular enclosure (30 cms x 12 cms x 30 cms) with rectangular aperture (20 cms x 3 cms) as shown in Figure 4 is determined as a function of frequency and presented in Figure 4 along with earlier published data [3]. It may be observed from the data presented in Figure 4 that numerical results obtained by the simple transmission line model used in [3] predicts less electric field shielding than the present method. However, the location of minimum shielding predicted by the present methods agrees better with the measured data compared to transmission line model of [3].

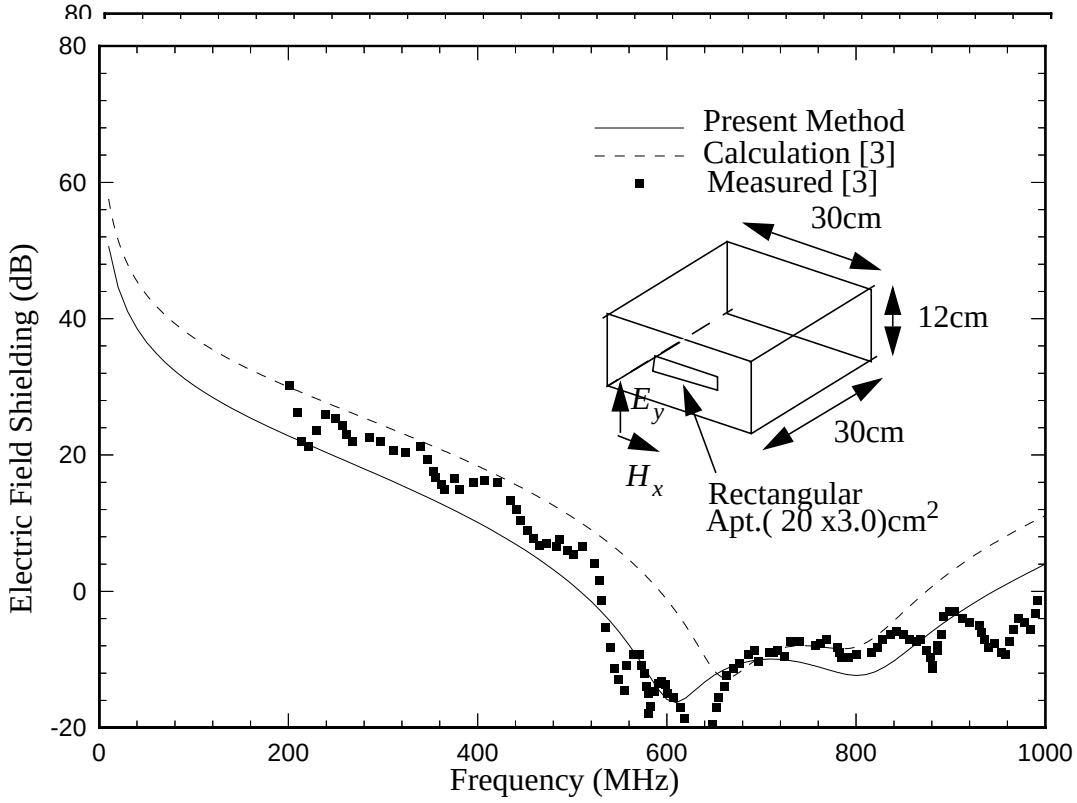

Figure 4 Electric field shielding at the center of (30 x 12 x 30) cm^3 enclosure with (20 x 3.0) cm^2 aperture located at 15 x 6 cm in z=0 plane

In the numerical data presented in Figure 4 only a single mode (i.e. $p = 1, q = 0$) over the aperture and dominant mode inside the cavity were considered. To study the effects of higher order cavity modes on the electric field shielding, a numerical example with the cavity and aper-

ture sizes same as shown in Figure 4 is considered. The electric field shielding calculated at the center of the rectangular enclosure considering maximum value of m equal to 100 and maximum value of n equal to 100 is shown in Figure 5 along with other numerical data. From the numerical data presented in Figure 5 it may be concluded that inclusion of higher order cavity modes improves electric field shielding estimation.

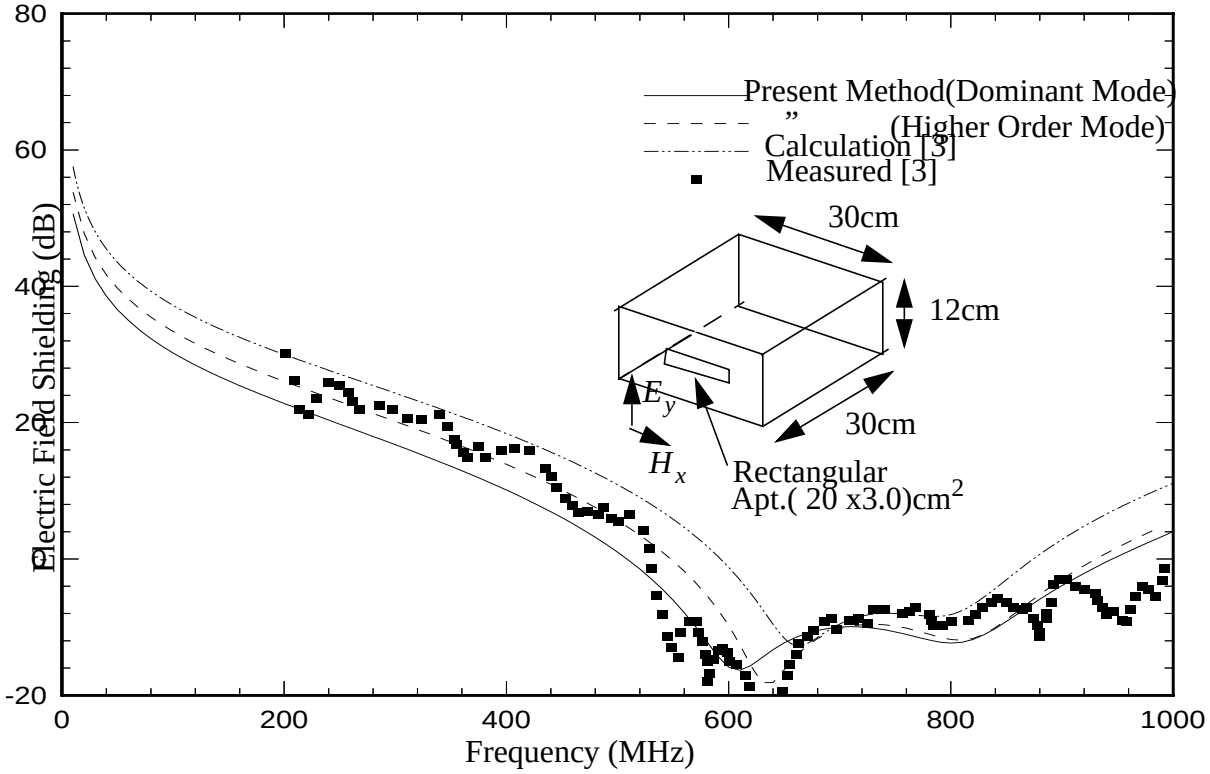

Figure 5 Electric field shielding at the center of (30 x 12 x 30) cm^3 enclosure with (20 x 3.0) cm^2 aperture located at 15 x 6 cm in z=0 plane

Figures 6 and 7 show the electric field shielding when more than a single mode is considered at the aperture. The dimensions of the enclosure and the rectangular aperture for Figures 6 and 7 were the same as shown in Figure 4. From Figures 6 and 7 it may be concluded that for the

aperture size and the frequency range considered, a single dominant mode at the aperture is adequet for achieving convergent results.

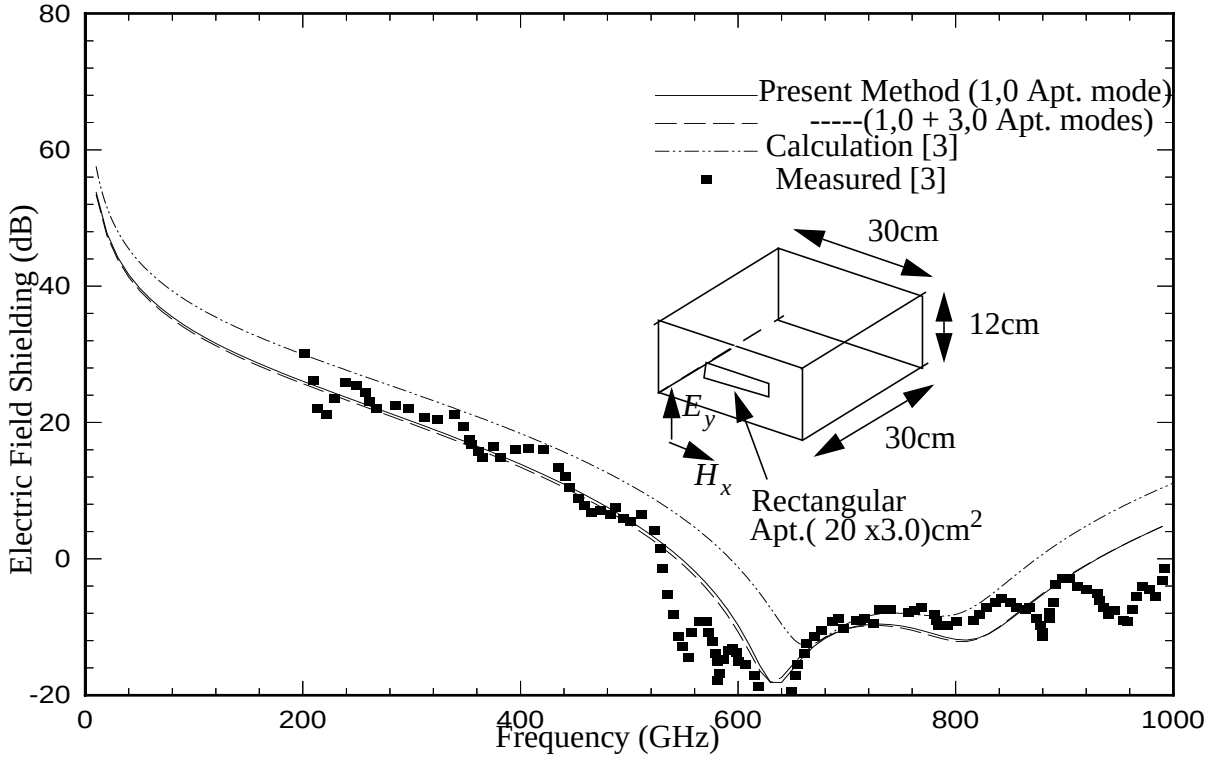

Figure 6 Electric field shielding at the center of (30 x 12 x 30) cm^3 enclosure with (20 x 3.0) cm^2 aperture located at 15 x 6 cm in z=0 plane

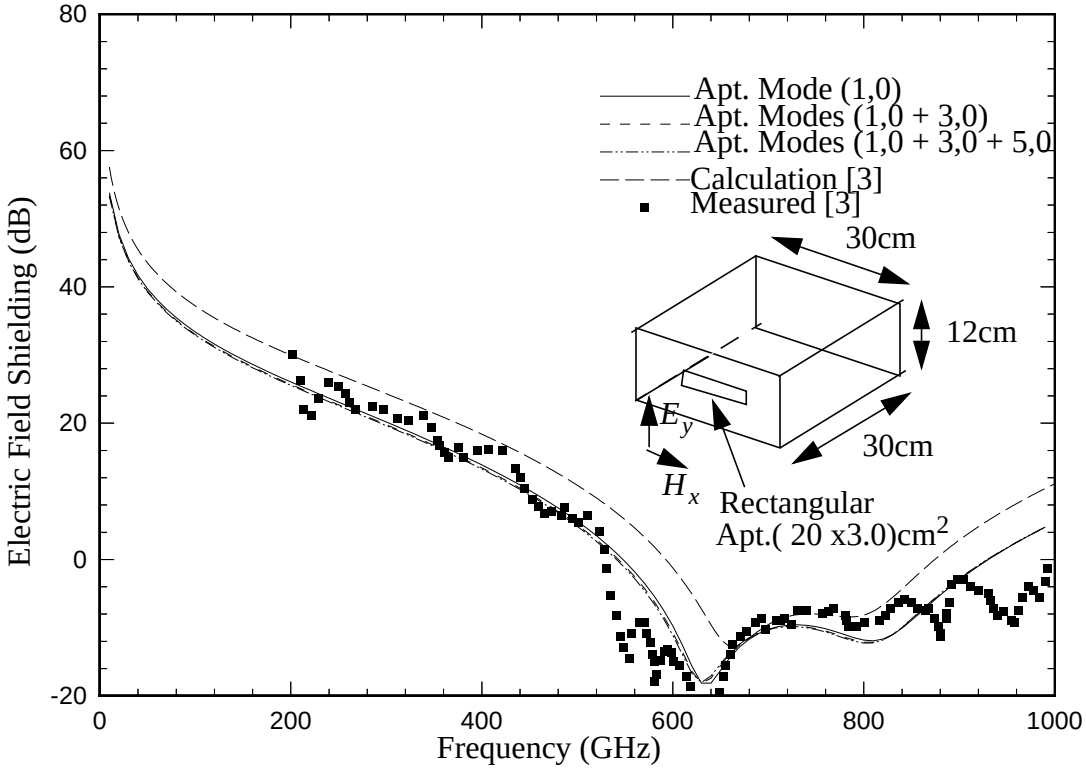

Figure 7 Electric field shielding at the center of (30 x 12 x 30) cm^3 enclosure with (20 x 3.0) cm^2 aperture located at 15 x 6 cm in z=0 plane

3.2 Two Aperture Case

Consider a rectangular enclosure with two rectangular apertures, one on the $z = 0$ and another on the $z = c$ planes. It is assumed that the enclosure is illuminated by a plane wave at normal incidence on the aperture at the $z = 0$ plane. Due to assumed polarization of the incidence wave it can be shown that $V_{rpq} = 0$ and $A_{rpq} = 0$. Hence the matrix equation (92) reduces to

$$\begin{bmatrix} Y^{x1x1}_{rpqr'p'q'} & Y^{x1x2}_{rpqr'p'q'} \\ Y^{x2x1}_{rpqr'p'q'} & Y^{x2x2}_{rpqr'p'q'} \end{bmatrix} \begin{bmatrix} U_{rpq} \\ B_{rpq} \end{bmatrix} = \begin{bmatrix} I_{r'p'q'xi} \\ 0 \end{bmatrix} \tag{96}$$

The matrix equation (96) is solved for U_{rpq} and B_{rpq} using numerical methods. From U_{rpq} and B_{rpq} the electric field shielding can be determined using expression (93). For numerical solution of (96) we consider a rectangular cavity with $a = 30$ cms, $b = 12$ cms, and $c = 30$ cms with two rectangular apertures. One of the rectangular apertures was of size $(20x3.0)$ cm^2, located at 15, 6, 0 cms, and another rectangular aperture of the same size as the first aperture but located at 15, 6, 30 cms. The rectangular cavity is illuminated by plane wave at normal incidence to the first aperture. Assuming only $p = 1, q = 0$ expansion mode on the aperture and considering only dominant $m = 1, n = 0$ mode inside the cavity, the electric field shielding obtained using the present method is plotted in Figure 8 (Solid Line). The numerical data represented by the solid line in Figure 8 is obtained with the internal coupling between the apertures not zero (i.e. setting $Y^{x2x1}_{rpqr'p'q'} \neq Y^{x1x2}_{rpqr'p'q'} \neq 0$). The electric field shielding of the rectangular enclosure with two apertures is also obtained by extending the simple transmission line model described in [3]. In this model the expression for Z_3 given in equation (6) of reference [3] is modified to

$$Z_3 = Z_g \frac{(Z_{ap} + jZ_g \tan(k_g(d-p)))}{Z_g + jZ_{ap}\tan(k_g(d-p))} \tag{97}$$

to account for the second aperture. The numerical data obtained using the simple transmission line are also plotted in Figure 8. General behaviour of the electric field shielding as a function of frequency obtained by the present method and the transmission line method [3] is in good agreement. It is also observed that when the mutual coupling between the apertures is not considered the present method gives shielding results identical to the results obtained using transmission line

method.

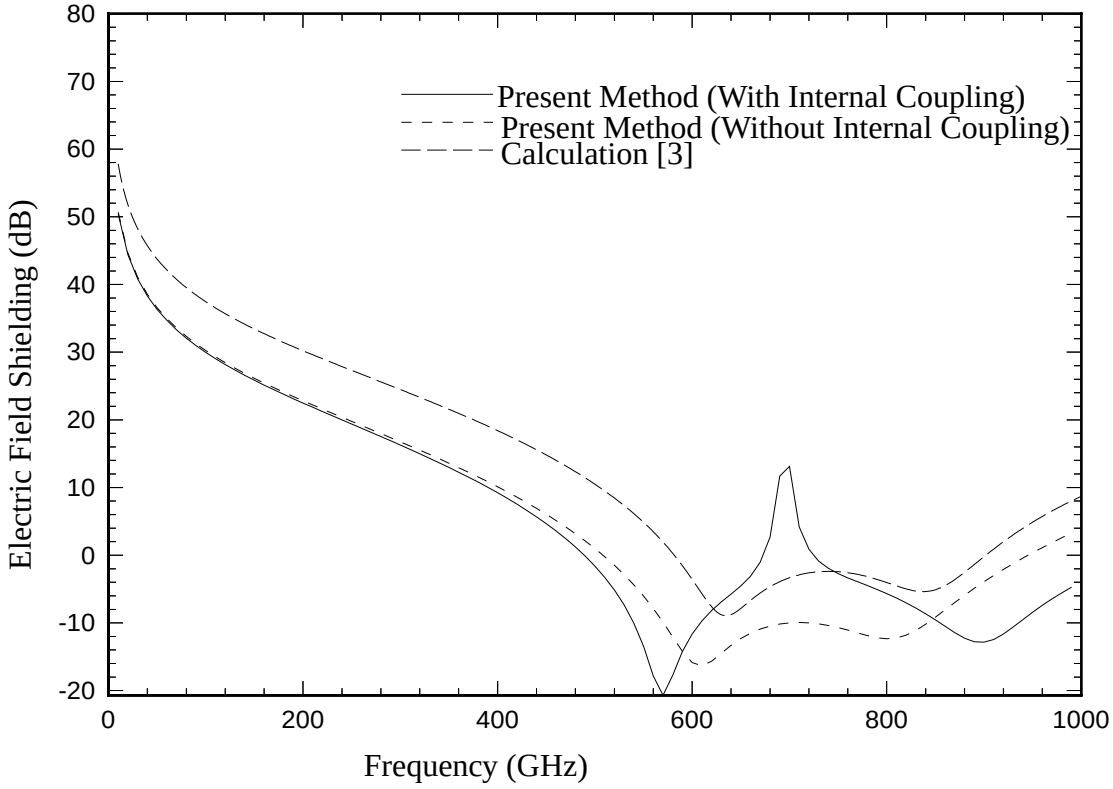

Figure 8 Electric field shielding at the center of (30 x 12 x 30) cm^3 enclosure with two identical apertures with (20 x 3.) cm^2 size. Aperture one located at (15 ,6 , 0) cms, aperture two located at (15, 6 , 30) cms.

In Figure 9 the electric field shielding for the enclosure and aperture dimensions as given in Figure 8 is studied when higher order modes inside the cavity and on the apertures are considered.

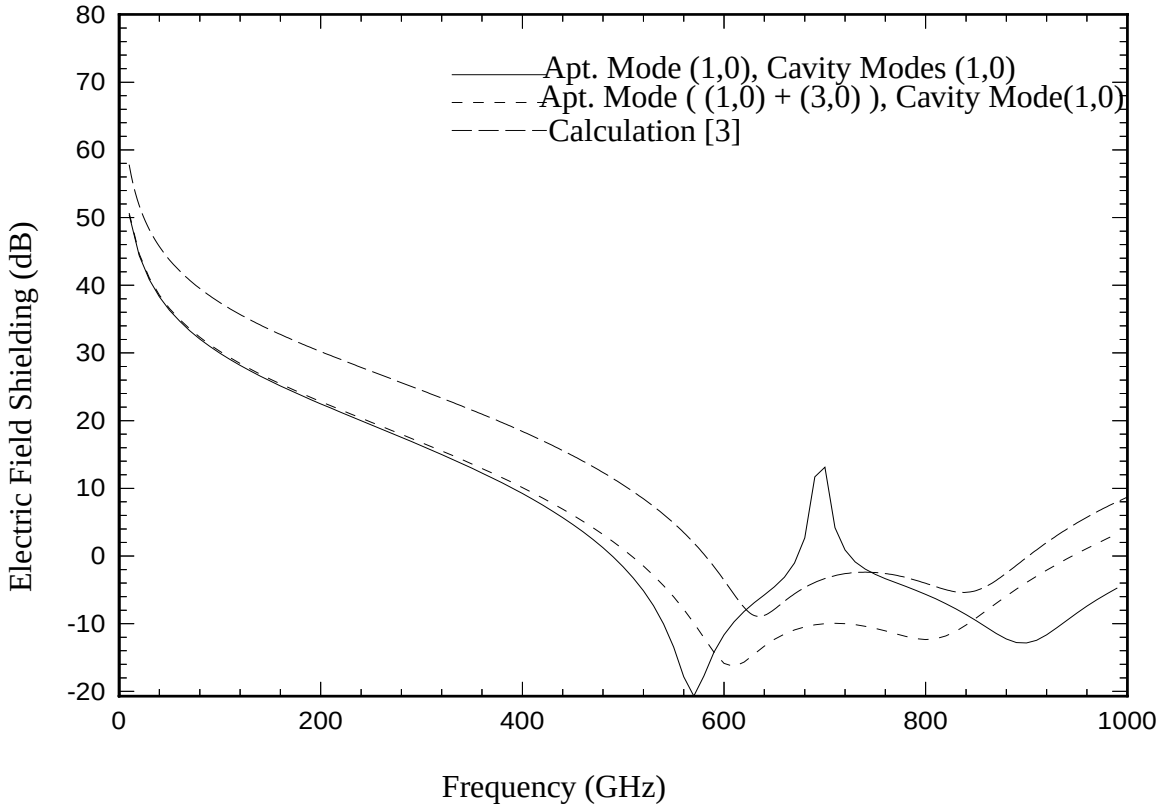

Figure 9(a) Effect of higher order aperture modes on electric field shielding at the center of (30 x 12 x 30) cm^3 enclosure with two identical apertures with (20 x 3.) cm^2 size. Aperture one located at (15 , 6 , 0) cms, aperture two located at (15 , 6 , 30) cms.

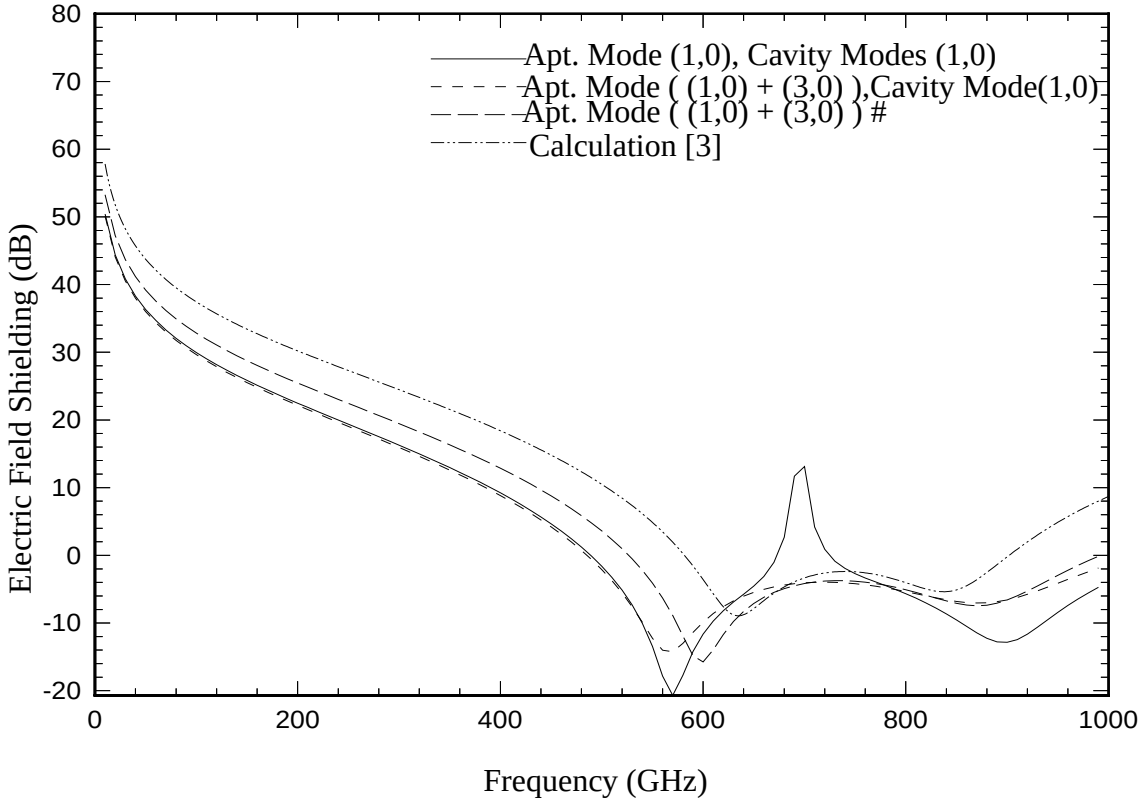

Figure 9(b) Effect of higher order aperture modes on electric field shielding at the center of (30 x 12 x 30) cm^3 enclosure with two identical apertures with (20 x 3.) cm^2 size. Aperture one located at (15 , 6 , 0) cms, aperture two located at (15 , 6 , 30) cms. # Cavity modes considered (100 x100).

To validate the Modal Method (MM) presented in this report, in the following section, we compare the electric field shielding data obtained using the MM method with the FEM-MoM [8] techniques. For numerical simulation we consider a rectangular cavity with $a = 30$ cms, $b = 12$ cms, and $c = 30$ cms with two rectangular apertures. One of the rectangular apertures was of size $(20x3.0)$ cm^2, located at 15, 6, 0 cms, and another rectangular aperture of the same size as the first aperture but located at 15, 6, 30 cms. The rectangular cavity is illuminated by a plane wave at normal incidence to the first aperture. Assuming two aperture modes and m-max =

100, and n-max = 100, the electric field shielding at the center of the cavity is calculated using the present method and presented in Figure 10. In Figure 10, the numerical data on electric field shielding of the cavity using the hybrid Finite Element Method-Method of Moments (FEM/MoM) [8] is also presented for various sizes of the apertures. Eexcellent agreement between the results obtained from the present and FEM/MoM methods validates the accuracy of the present method.

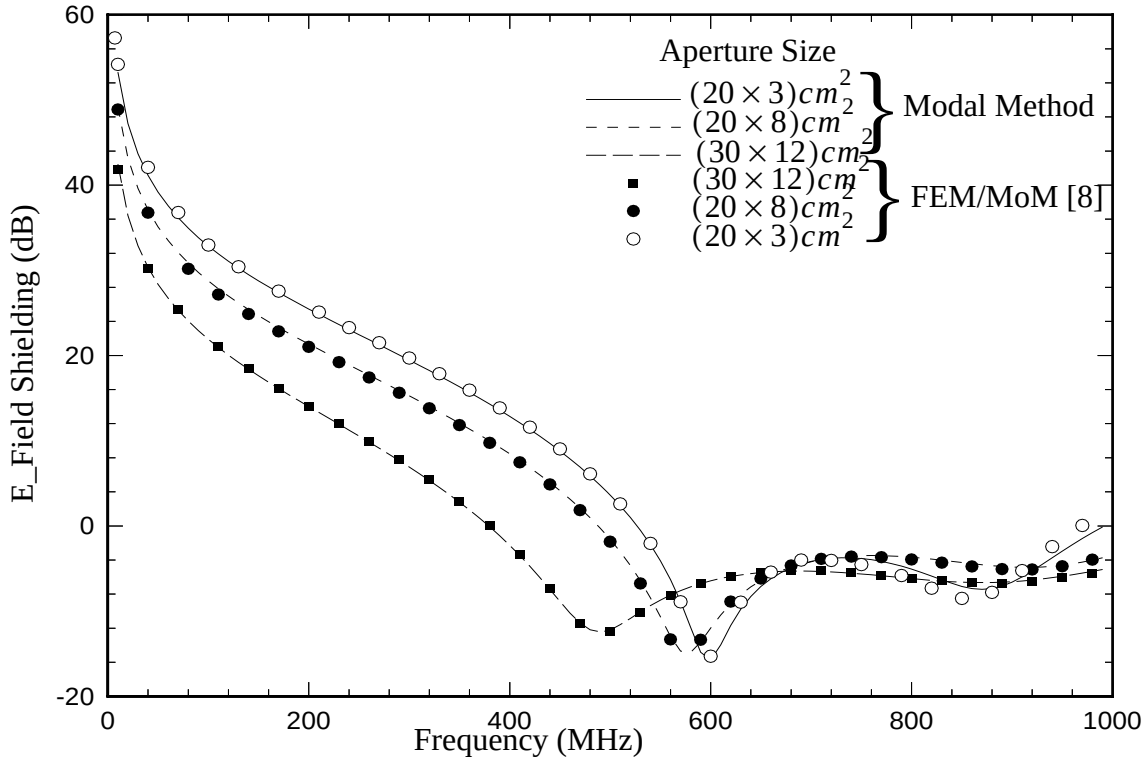

Figure 10 Electric field shielding of rectangular enclosure of size (30 x 12 x 30) cm3 with two identical rectangular apertures (one on each side) of various sizes when illuminated by incident plane wave at normal incidence.

Figure 11 shows a rectangular cavity excited through four apertures; two on each side. The cavity and aperture sizes used in Figure 11 are small enough so that shielding effectiveness of the cavity can be calculated using FEM/MoM for validation purpose. The electric field shielding of the cavity shown in Figure 11 is calculated using the present and FEM/MoM methods and pre-

sented in Figure 12. A good agreement between the two results further validate the present method. The small disagreement at higher frequencies between the two methods may be attributed to the numerical inaccuracy involved in the FEM/MoM methods due to discretization level.

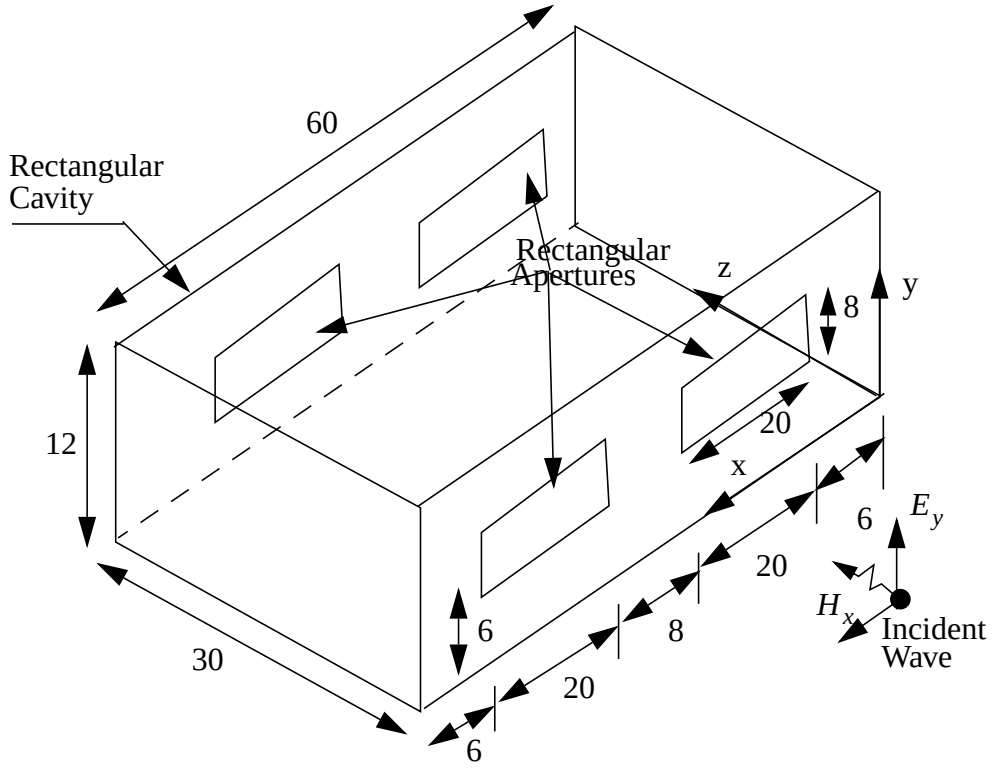

Figure 11 Rectangular cavity with four identical apertures and illuminated by plane wave with normal incidence. All dimensions in cm

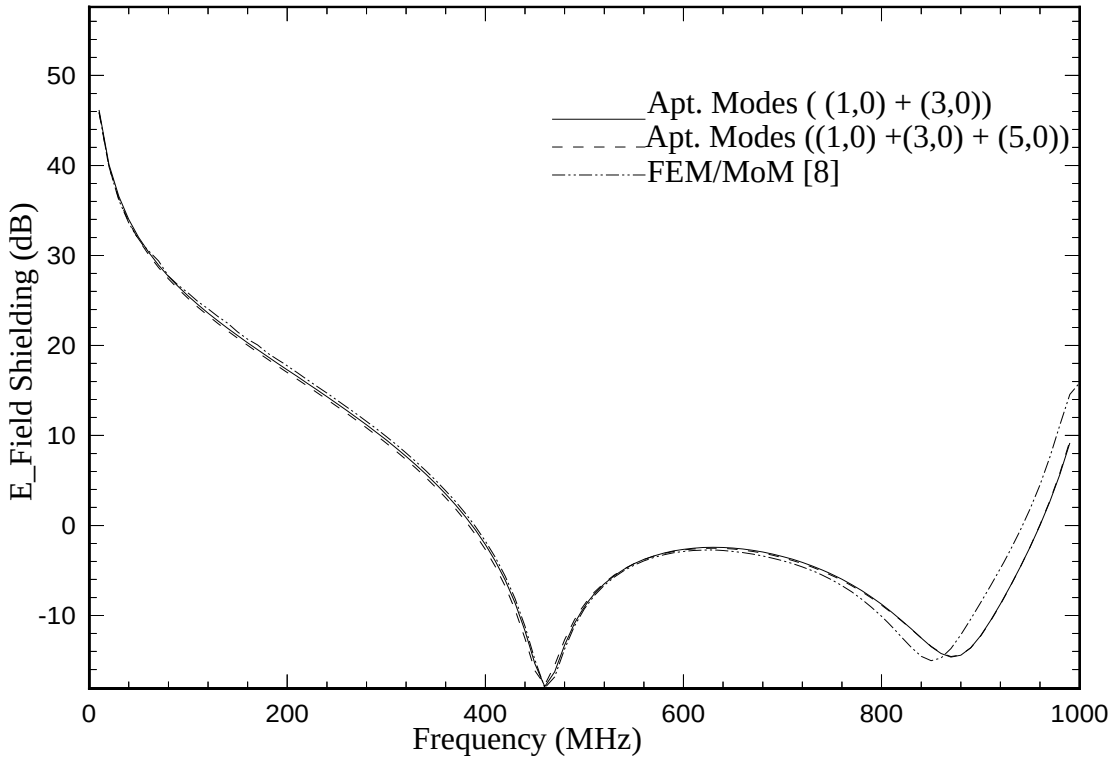

Figure 12 Electric field shielding of rectangular cavity shown in Figure 11. Observation point (30 , 6, 15) cm.

3.3 EM Field Penetration Inside B-757 Aircraft Configuration

A typical cross section of a B-757 aircraft with various dimensions is shown in Figure 13. For simplicity, the inner complexities of passenger seat arrangement and overhead compartments are assumed not to be present. The cross section shown in Figure 13 can be approximated by a rectangular crosssection as shown in Figure 13. Therefore the entire fuselage of a B-757 can be approximated by a rectangular cavity of dimensions shown in Figure 14(a). An external electromagnetic source would cause EM field to penetrate through passenger windows and cockpit windows into the fuselage. The EM field present inside the fuselage due to any external EM source may coupled to sensitive instrumentation wiring and hence cause electronic upset. Furthermore, if the EM field strength inside a fuselage is sufficiently large it may cause electric spark on broken

wires. It is therefore important to estimate electromagnetic field shielding of a B-757 fuselage or for that matter any aircraft passenger cabin. The external EM field may also penetrate a B-757 fuselage through the cockpit windows. However for an aircraft illuminated from sides passenger windows will be dominant contributors. Hence in this report only side windows are considered. Approximating the B-757 fuselage by a rectangular cavity with rectangular apertures representing passenger windows the computer code developed here is used to determine the field strength inside the passenger cabin due to any external EM source. For the worst case scenario, it is assumed that the cavity is excited by an electromagnetic plane wave at normal incidence with veritcal as well as horizontal polarizations.

For the numerical estimate of electric field shielding of a B-757 fuselage, we first consider the effect of two windows, one on each side of a rectangular cavity (3600 x 400 x 400 cms) as shown in Figure 14(b). The window dimensions selected for the numerical simulation were (25 x 35) cm^2. The windows were assumed to be located with their centers at (1800 , 200 , 0.0) cms and (1800, 200, 400) cms. Using the computer code developed here, the electric field shielding calculated at (1800, 120, 200) cms as a function of frequency is presented in Figure 13. In the numerical simulation it is assumed that the incident wave is polarized in the y-direction. The numbers of cavity modes considered in this example were $m = 0, 1, 2, ...,1200$ and $n = 0, 1, 2, ...200$. Any further addition of cavity modes was found to have no appreciable effect on the shielding calculation. For the numerical results shown in Figure 15 only a single dominant mode (i.e. $p = 1, q = 0$ was considered on the window apertures. For comparison, the measured values of electric field shielding for a B-757 aircraft at two separate frequencies are also shown in Figure 15. However, these measurements were done under different incident wave conditions and hence are shown here only for illustrating that the numerical data obtained using

the present method are in the range of measured values.

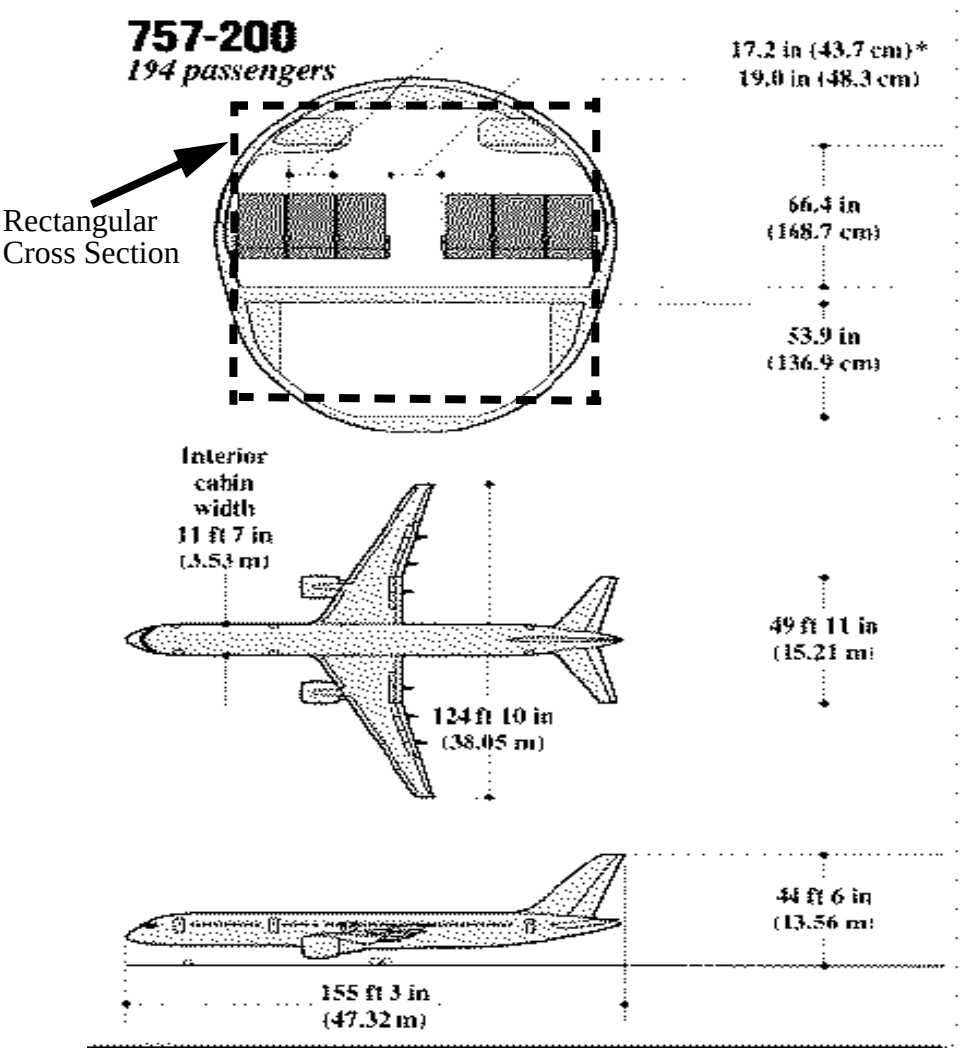

Figure 13 Geometry of B-757 aircraft configuration with cross sectional and longitudinal view. Dotted line shows approximated cross section.

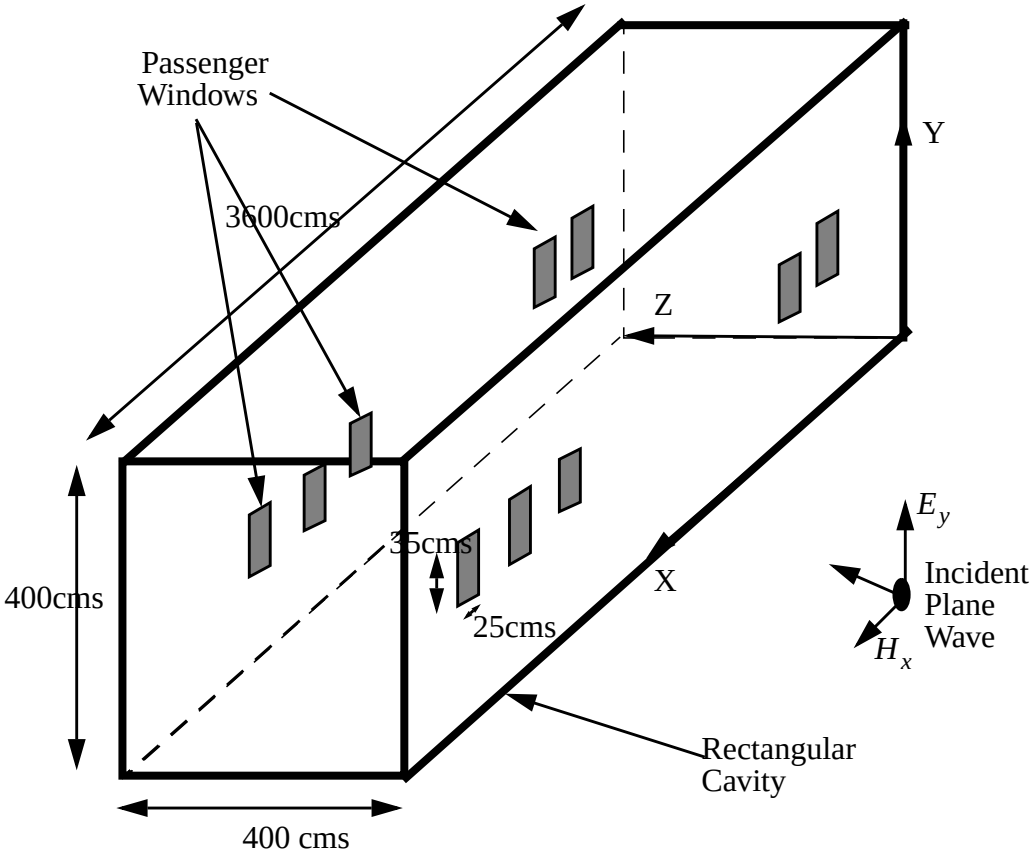

Figure 14(a) Closed rectangular cavity approximating B-757 fuselage with rectangular apertures on side walls representing passenger windows.

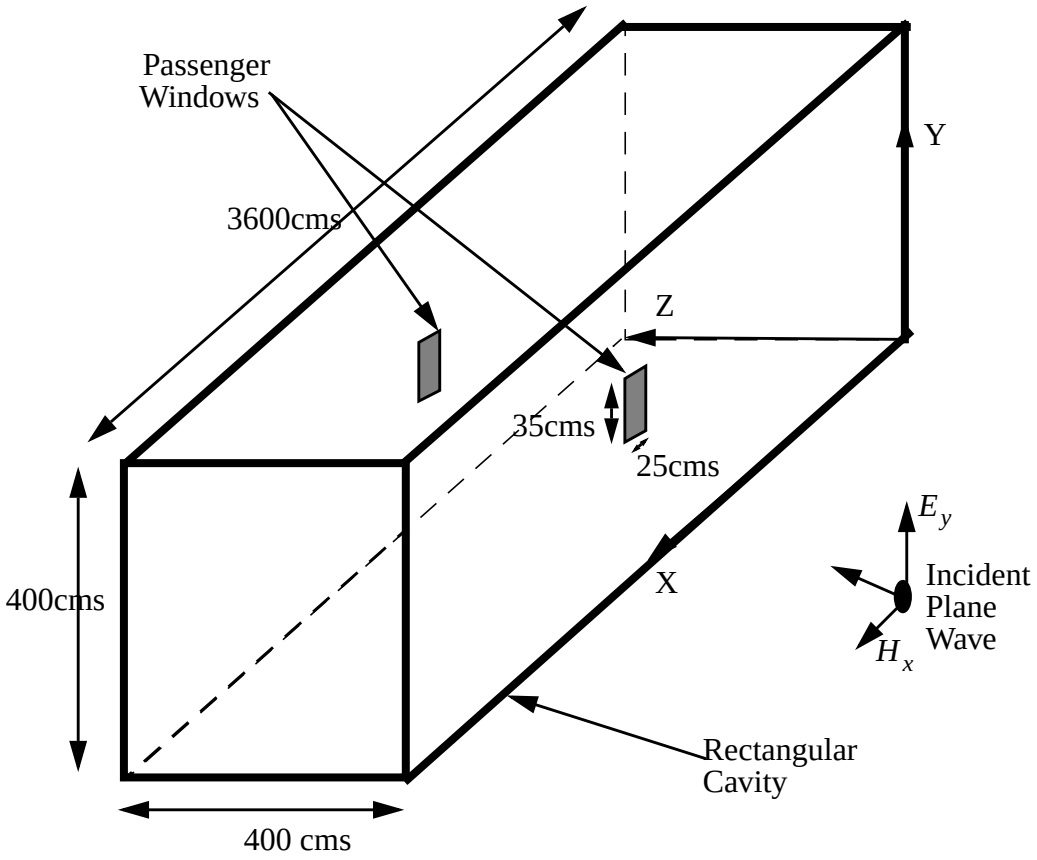

Figure 14(b) Closed rectangular cavity approximating B-757 fuselage with two rectangular apertures on side walls representing passenger windows.

Figures 15-17 shows the electric field shielding when higher order modes on the apertures were considered. In Figures 15-17, the incident wave was considered to be parallel to the longer dimensions of the aperture windows. For the frequency range shown in Figures 15-17 it is clear that single $p = 1, q = 0$ mode on the aperture is adequate for obtaining convergent results. Figure 18 shows the electric field shielding of a rectangular cavity with two apertures when the incident wave was polarized parallel to the shorter dimension of the window. The dimensions of the

cavity and aperture used in numerical data shown in Figure 18 were the same as given in Figure 15. Only a single aperture mode was considered in the numerical data shown in Figure 18.

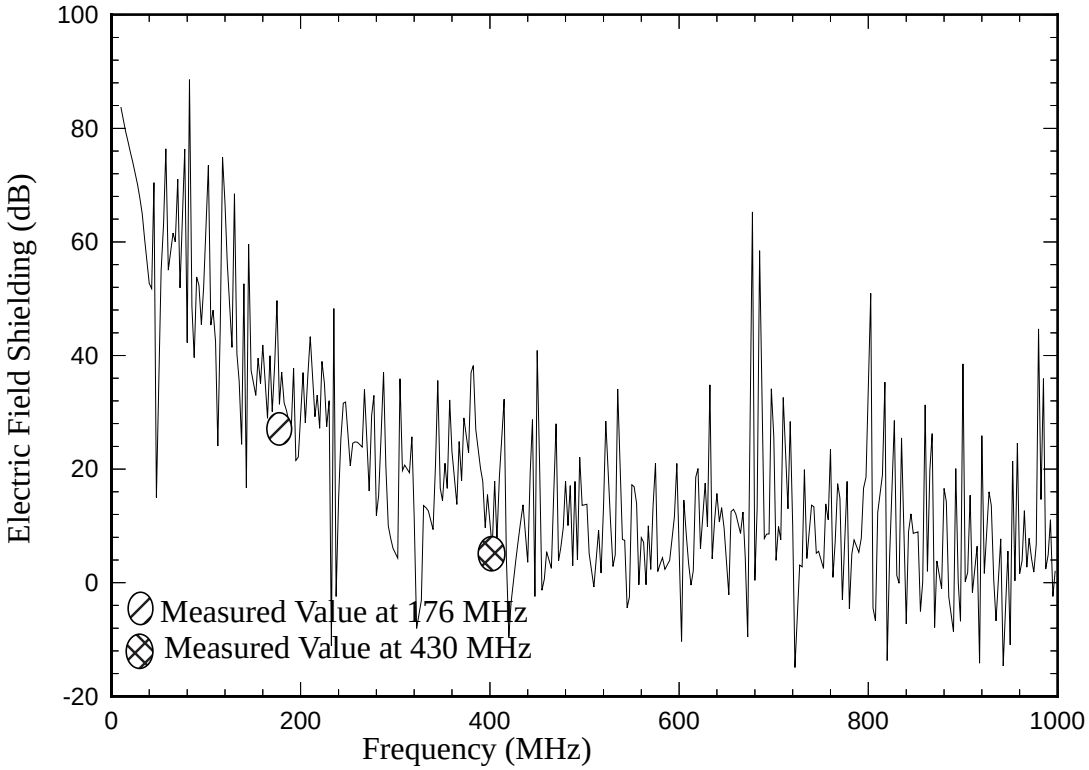

Figure 15 Electric field shielding of rectangular cavity approximating fuselage of B-757 aircraft. Two windows on each side of cavity were considered. Cavity size (3600 x 400 x 400) cm^3, window size (25 x 35) cm^2, window locations (1800, 200, 0.0) cms and (1800, 200, 400) cms. Field point location (1800, 120, 200) cms.

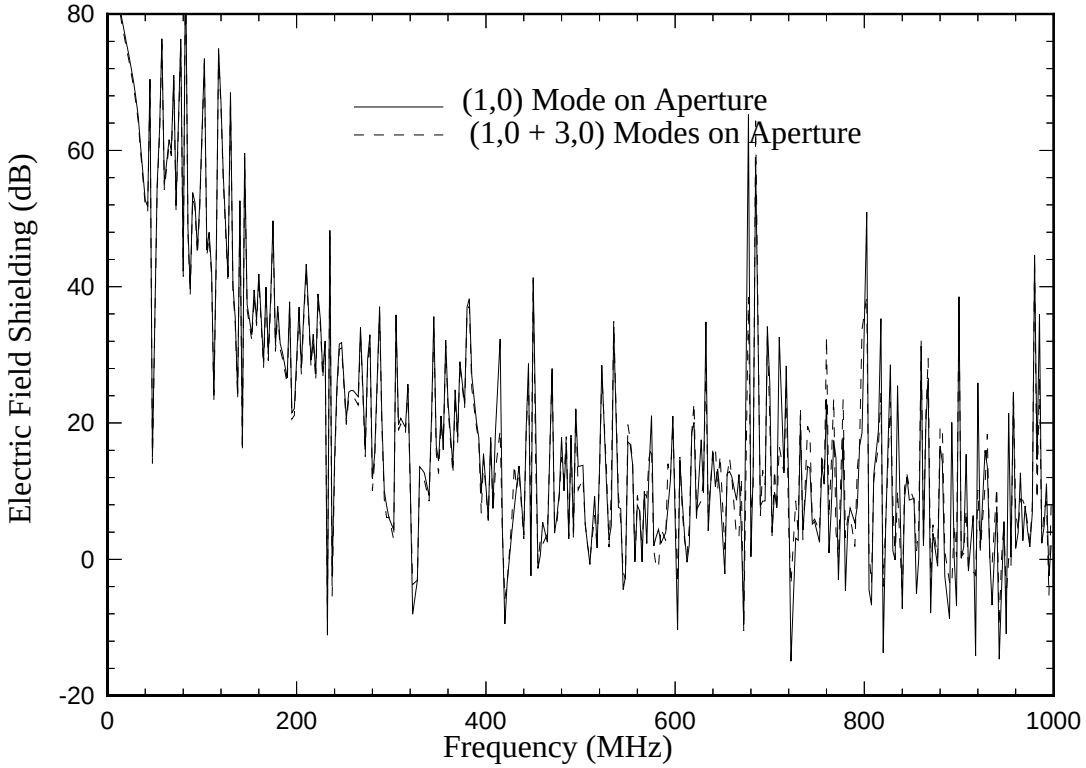

Figure 16 Electric field shielding of rectangular cavity approximating fuselage of B-757 aircraft. Two windows on each side of cavity were considered. Dimensions of Cavity, aperture and field point are as given in Figure 15

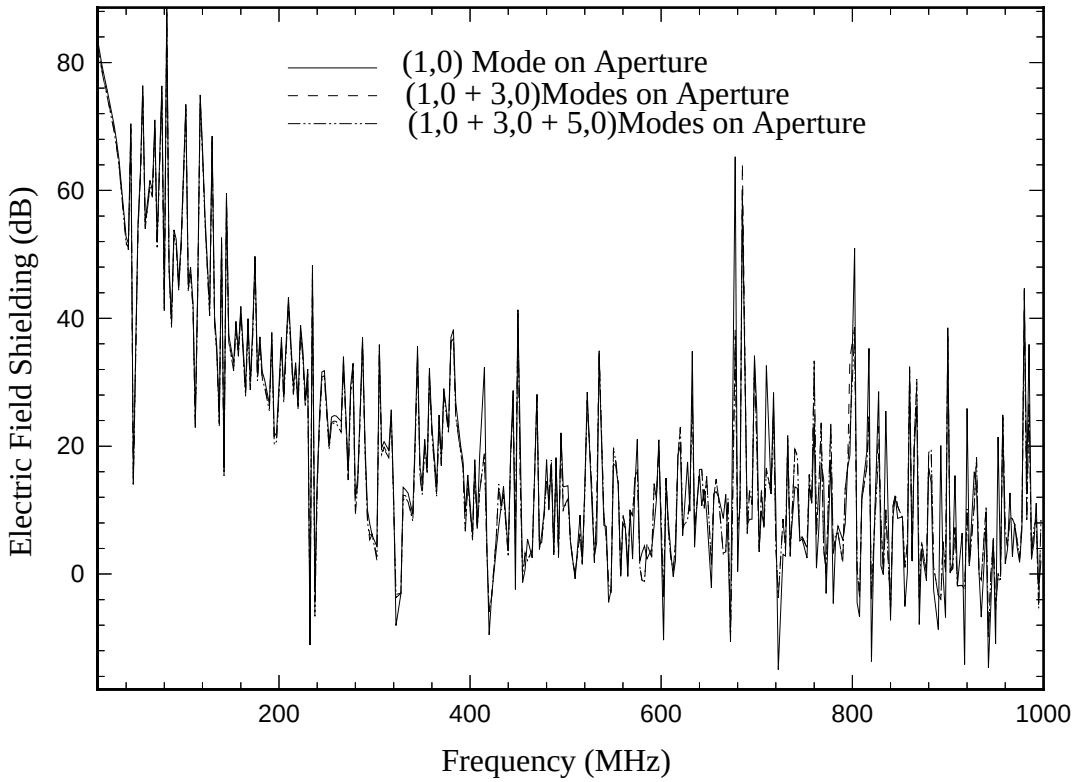

Figure 17 Electric field shielding of rectangular cavity approximating fuselage of B-757 aircraft. Two windows on each side of cavity were considered. Dimensions of cavity, aperture and field point are as given in Figure 15

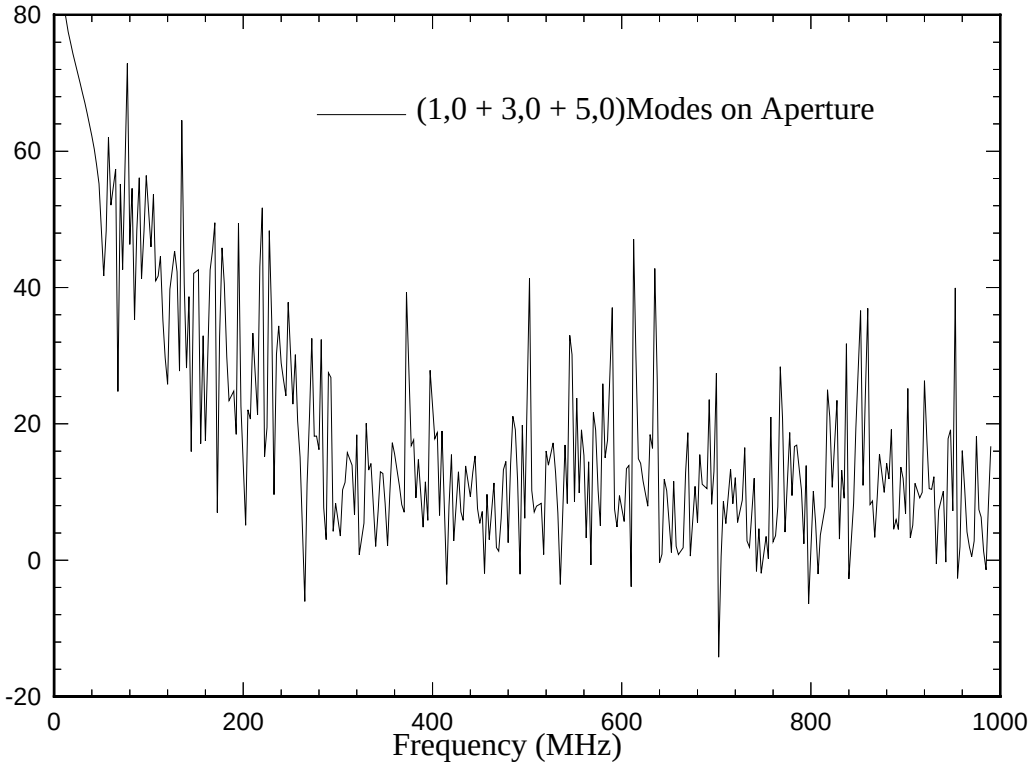

Figure 18 Electric field shielding (for horizontal polarization) of rectangular cavity approximating fuslelage ofB-757 aircraft. Two windows on each side of cavity were consideredDimensions of cavity, aperture and field point are as given in Figure 15

3.4 Convergence Test For Large size Cavities

The numerical estimate of electric field shielding in an electrically large size cavities illuminated through large size the apertures depends upon the number of cavity modes as well as aperture modes considered in the numerical simulation. An adequate number of cavity modes and aperture modes must be considered to achieve numerical stable results. In this section, dependence of the electric field shielding on number of cavity modes and aperture modes is studied through numerical examples.

For numerical estimate of electric field shielding, we first consider a rectangular cavity

(5400 x 600 x 600) cm^3, which approximates the fuselage of a Boeing-747. For numerical simulation only two windows; one on each side of fuselage were considered. The aperture dimensions selected for the numerical simulation were (25 x 35) cm^2. The window was assumed to be located with their centers at (2700, 300, 0.0) cms and (2700, 300, 600) cms. Using the computer code developed here, the electric field in volts/meter calculated at (2700, 300, 300) cms as a function of mode index n is presented in Figure 19. In the numerical simulation it is assumed that the incident wave is polarized in the y-direction. In Figure 19, stable results are obtained for the cavity mode index n higher than 200. For Figure 19, only a single mode at the aperture was considered.

For the cavity and window dimensions as shown in Figure 19, the electric field at the center of cavity is calculated and shown in Figure 20 as a function of cavity mode index m. From Figure 20 it is clear that $m \geq 1200$ achieves numerically stable results.

After selecting the cavity mode indices m, n for numerically stable results, the electric field at the center of the cavity with dimensions as shown in Figure 19 is calculated as a function of aperture modes and shown in Figure 21. From Figure 21 it may be concluded that for normal incidence the 4 or 5 aperture modes are sufficient to obtain numerically stable results. Consideration of higher order modes on the aperture improves the accuracy of the numerical calculation but increases the computational time significantly. For fast computation of electric field shielding, we consider only single mode at the aperture.

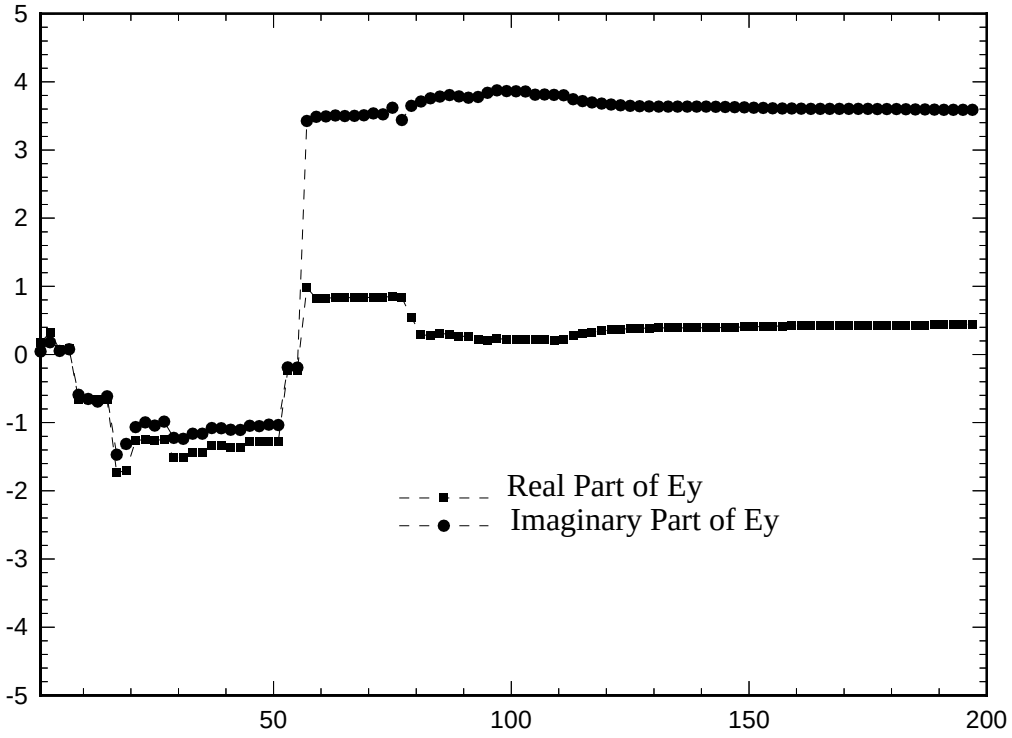

Figure 19 Electric field amplitude at (2700, 300, 300) cms inside a rectangular cavity (5400x600x600) cm^3 illuminated by plane wave at normal incidence through rectangular windows (25 x 35) cm^2 as a function of cavity mode index n. Other parameters: cavity mode index m = 1200, frequency = 2.87510864 GHz.

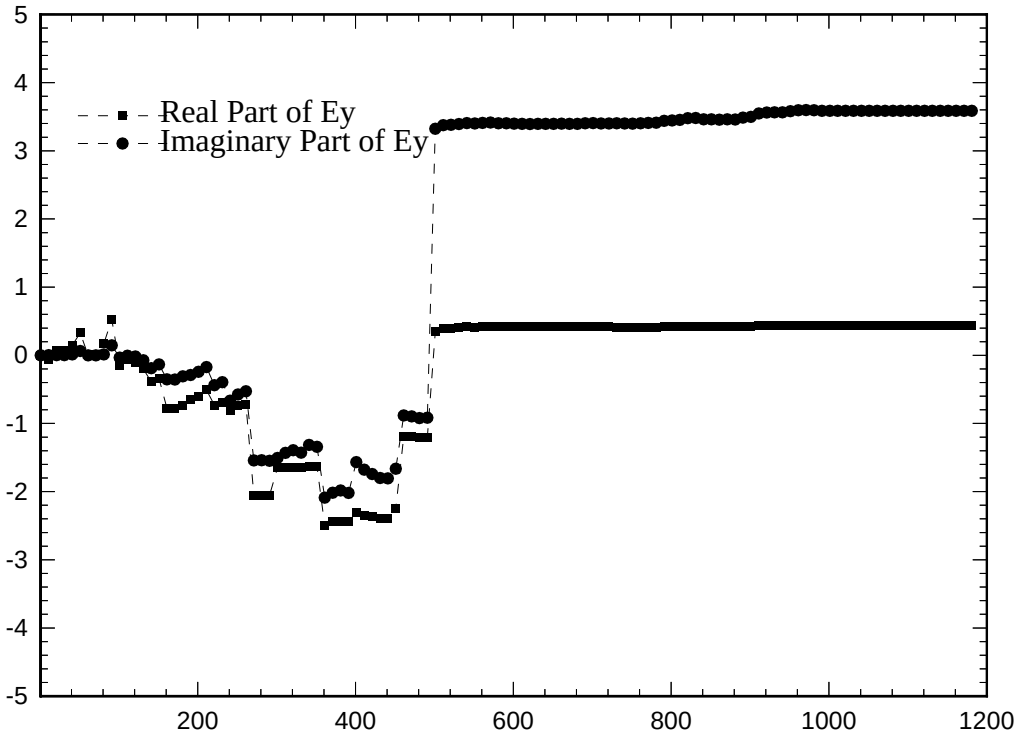

Figure 20 Electric field amplitude at (2700, 300, 300) cms inside a rectangular cavity (5400x600x600) cm^3 illuminated by plane wave at normal incidence through rectangular windows (25 x 35) cm^2 as a function of cavity mode index m. Other parameters: cavity mode index n = 200, frequency = 2.87510864 GHz.

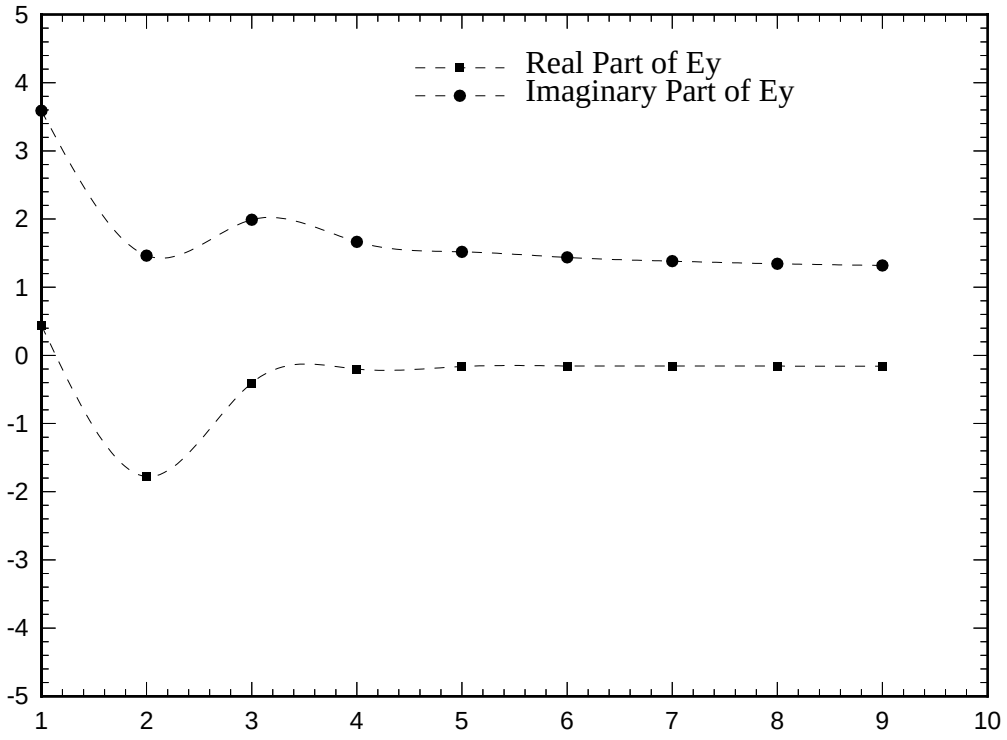

Figure 21 Electric field amplitude at (2700, 300, 300) cms inside a rectangular cavity (5400x600x600) cm^3 illuminated by plane wave at normal incidence through rectangular windows (25 x 35) cm^2 as a function of number of modes on apertures. Other parameters are cavity mode index n = 200, m = 1200, frequency = 2.8745GHz.

4.0 Conclusion

A method suitable for estimation of electric field shielding effectiveness of large but regular shaped rectangular cavity with multiple rectangular apertures is presented. Assuming appropriate electric field distribution on the aperture, fields inside the cavity are determined using rectangular cavity Green's function. Electromagnetic fields outside the cavity and scattered due to the aperture are obtained using the free space Green's function. Matching the tangential magnetic field across the apertures, the integral equation with aperture fields as unknown variables is obtained. The integral equation is solved for unknown aperture fields using the Method of Moments. From the aperture fields the electromagnetic shielding effectiveness of the rectangular cavity is determined.

Numerical results on electric field shielding of a rectangular enclosure are validated with data available in the literature. Effects of cavity and aperture modes for large size enclosure are studied. Approximating a Boeing-757 aircraft cabin by a rectangular cavity and passenger windows by rectangular aperture electromagnetic field penetrations inside the cabin due to external plane wave at normal incidence are estimated. Electromagnetic field penetrations due to horizontal as well as vertical polarizied incident fields are studied. Though in the present report electromagnetic field penetration through two apertures, one on each side of fuselage is estimated, the computer code can be used to simulate effects of multiple apertures on each side of fuselage.

One advantage of the present method is that the order of matrix equation to be solved in the present approach is very small compared to the order of matrix equation one encounters in the Finite Element Method. Another advantage is that the computer storge requirement for the present approach is negligibly small compared to the Finite Element Method and Finite Difference Time Domain method. However, because of the use of the cavity Green's function it is very

difficult to take into account the complex geometries and objects that may be present in the passenger cabins. Also, the method does not take into account the losses that will be present in practical aircraft cabin. Inspite of its inadequateness in handling losses in the system and complex geometries, the present method gives quick and fairly accurate estimates of electromagnetic shielding effectiveness of rectangular enclosures.

Acknowledgement

The author is grateful to Dr. C. J. Reddy, Hampton University, Hampton, Virginia, for providing FEM /MoM numerical results shown in Figures 10 and 12.

References

[1] H. A. Mendez, " Shielding theory of enclosures with apertures, " IEEE Trans. on Electromagnetic Compatibility, Vol. EMC -20, No. 2, pp. 296-305, May 1978.

[2] G. Cerri, R. D. Leo, and V. M. Primiani, " Theoretical and experimental evaluation of the electromagnetic radiation from apertures in shielded enclosures, " IEEE Trans. on Electromagnetic Compatibility, Vol. EMC -34, No. 4, pp. 423-432, Nov. 1992.

[3] M. P. Robinson, et al., "Analytical formulation for the shielding effectiveness of enclosures with apertures, " IEEE Trans. on Electromagnetic Compatibility, Vol. EMC-40, No. 3, pp. 240-247, August 1998.

[4] M. P. Robinson, et al., "Shielding effectiveness of a rectangular enclosure with a rectangular aperture, " Electronics Letter, Vol. 32, No. 17, pp. 1559-1560, 15th August 1996.

[5] D. A. Hill, et al., "Aperture excitation of electrically large, lossy cavities, " IEEE Trans. on Electromagnetic Compatibility, Vol. EMC 36, No. 3, pp. 169-178, August 1994.

[6] K. S. Kunz and R. J. Luebbers, "The finite difference time domain methods for electromagnetics, " Orlando, FL, CRC, 1993.

[7] C. J. Reddy et al., "A combined FEM/MoM/GTD technique to analyze elliptically polarized cavity-backed antenna with finite ground plane, " NASA Technical Paper 3618, Nov. 1996.

[8] C. J. Reddy and M. D. Deshpande, “User’s Manual for CBS3DS Version 1.0, ” NASA Contractor Report 198236, Oct. 1995.

Appendix I

In this appendix we evaluate the integral $\iint \Psi_{rpqx}(x', y') \sin\left(\frac{m\pi x'}{a}\right) \cos\left(\frac{n\pi y'}{b}\right) dx'dy'$ in a closed form. Substituting for $\Psi_{rpqx}(x', y')$ the expression for I_{rpqmnx} can be written as

$$\int_{-\frac{W_r}{2}}^{\frac{W_r}{2}} \int_{-\frac{L_r}{2}}^{\frac{L_r}{2}} \sin\left(\frac{p\pi}{L_r}\left(\frac{L_r}{2} + x'\right)\right) \cos\left(\frac{q\pi}{W_r}\left(\frac{W_r}{2} + y'\right)\right) \sin\left(\frac{m\pi(x' + x_r)}{a}\right) \cos\left(\frac{n\pi(y' + y_r)}{b}\right) dx'dy'$$

In above equation x_r, y_r are the coordinates of the center of r^{th} aperture. Performing the integration expression for I_{rpqmnx} can be written as

$$-\frac{p\pi L_r}{(p\pi)^2 - \left(\frac{m\pi L_r}{a}\right)^2} \left\{ \cos(p\pi) \sin\left(\frac{m\pi}{a}\left(\frac{L_r}{2} + x_r\right)\right) + \sin\left(\frac{m\pi}{a}\left(\frac{L_r}{2} - x_r\right)\right) \right\}$$

$$\frac{-(n\pi)/b}{\left(\frac{q\pi}{W_r}\right)^2 - \left(\frac{n\pi}{b}\right)^2} \left\{ \cos(q\pi) \sin\left(\frac{n\pi}{b}\left(\frac{W_r}{2} + y_r\right)\right) + \sin\left(\frac{n\pi}{b}\left(\frac{W_r}{2} - y_r\right)\right) \right\} \quad (98)$$

Appendix II

In this appendix we evaluate the integral $\iint \Phi_{rpqy}(x', y') \cos\left(\frac{m\pi x'}{a}\right) \sin\left(\frac{n\pi y'}{b}\right) dx'dy'$ in a closed form. Substituting for $\Phi_{rpqy}(x', y')$ the expression for I_{rpqmny} can be written as

$$\int_{-\frac{W_r}{2}}^{\frac{W_r}{2}} \int_{-\frac{L_r}{2}}^{\frac{L_r}{2}} \cos\left(\frac{p\pi}{L_r}\left(\frac{L_r}{2} + x'\right)\right) \sin\left(\frac{q\pi}{W_r}\left(\frac{W_r}{2} + y'\right)\right) \cos\left(\frac{m\pi(x' + x_r)}{a}\right) \sin\left(\frac{n\pi(y' + y_r)}{b}\right) dx'dy'$$

In above equation x_r, y_r are the coordinates of the center of r^{th} aperture. Performing the integration expression for I_{rpqmny} can be written as

$$-\frac{q\pi W_r}{(q\pi)^2 - \left(\frac{n\pi W_r}{b}\right)^2} \left\{ \cos(p\pi) \sin\left(\frac{n\pi}{b}\left(\frac{W_r}{2} + y_r\right)\right) + \sin\left(\frac{n\pi}{b}\left(\frac{W_r}{2} - y_r\right)\right) \right\}$$

$$\frac{-(m\pi)/a}{\left(\frac{p\pi}{L_r}\right)^2-\left(\frac{m\pi}{a}\right)^2}\left\{\cos(p\pi)\sin\left(\frac{m\pi}{a}\left(\frac{L_r}{2}+x_r\right)\right)+\sin\left(\frac{m\pi}{a}\left(\frac{L_r}{2}-x_r\right)\right)\right\} \tag{99}$$

Appendix III

The Fourier transforms ϕ_{rpqy} and ψ_{rpqx} of Φ_{rpqy} and Ψ_{rpqx}, respectively are derived in this appendix. Using the defination $\psi_{rpqx}(k_x, k_y) = \iint_r \Psi_{rpqy} e^{-jk_x x - jk_y y} dxdy$, the Fourier transform ψ_{rpqx} can be written as

$$\psi_{rpqx} = \frac{L_r W_r}{4j} e^{-jk_x x_r - jk_y y_r}\left\{e^{j\frac{p\pi}{2}}\frac{\sin\left(\frac{p\pi}{2}-\frac{k_x L_r}{2}\right)}{\frac{p\pi}{2}-\frac{k_x L_r}{2}} - e^{-j\frac{p\pi}{2}}\frac{\sin\left(\frac{p\pi}{2}+\frac{k_x L_r}{2}\right)}{\frac{p\pi}{2}+\frac{k_x L_r}{2}}\right\}$$

$$\left\{e^{j\frac{q\pi}{2}}\frac{\sin\left(\frac{q\pi}{2}-\frac{k_y W_r}{2}\right)}{\frac{q\pi}{2}-\frac{k_y W_r}{2}} + e^{-j\frac{q\pi}{2}}\frac{\sin\left(\frac{q\pi}{2}+\frac{k_y W_r}{2}\right)}{\frac{q\pi}{2}+\frac{k_y W_r}{2}}\right\}$$

Following the same procedure the Fourier transform of Φ_{rpqy} can be written as

$$\phi_{rpqy} = \frac{L_r W_r}{4j} e^{-jk_x x_r - jk_y y_r}\left\{e^{j\frac{p\pi}{2}}\frac{\sin\left(\frac{p\pi}{2}-\frac{k_x L_r}{2}\right)}{\frac{p\pi}{2}-\frac{k_x L_r}{2}} + e^{-j\frac{p\pi}{2}}\frac{\sin\left(\frac{p\pi}{2}+\frac{k_x L_r}{2}\right)}{\frac{p\pi}{2}+\frac{k_x L_r}{2}}\right\}$$

$$\left\{e^{j\frac{q\pi}{2}}\frac{\sin\left(\frac{q\pi}{2}-\frac{k_y W_r}{2}\right)}{\frac{q\pi}{2}-\frac{k_y W_r}{2}} - e^{-j\frac{q\pi}{2}}\frac{\sin\left(\frac{q\pi}{2}+\frac{k_y W_r}{2}\right)}{\frac{q\pi}{2}+\frac{k_y W_r}{2}}\right\}$$

The expressions for ψ^*_{rpqx} and ϕ^*_{rpqy} are obtained from expressions for ψ_{rpqx} and ϕ_{rpqy}, respectively by replacing k_x, k_y by $-k_x, -k_y$ respectively.

Appendix IV

In this appendix, the expressions for electric field inside the cavity due to magnetic current sources present on its walls are given. Using the electric vector potential given in (31) and expression (23), the electric field components inside the cavity due to the x component of magnetic current sources at $z = 0$ plane are obtained as

$$E_x^{IIx0} = 0$$

$$E_y^{IIx0} = \sum_{r=1}^{R} \sum_{p,q} U_{rpq} \sum_{m,n}^{\infty} \frac{1}{k_I} \frac{\varepsilon_{0m}\varepsilon_{0n}}{ab\sin(k_I c)} \left(k_0^2 - \left(\frac{n\pi}{b}\right)^2\right) \sin\left(\frac{m\pi x}{a}\right) \cos\left(\frac{n\pi y}{b}\right) \sin(k_I(c-z)) I_{rpqmnx}$$

$$E_z^{IIx0} = \sum_{r=1}^{R} \sum_{p,q} U_{rpq} \sum_{m,n}^{\infty} \frac{1}{k_I} \frac{\varepsilon_{0m}\varepsilon_{0n}}{ab\sin(k_I c)} \frac{n\pi}{b} \sin\left(\frac{m\pi x}{a}\right) \sin\left(\frac{n\pi y}{b}\right) \cos(k_I(c-z)) I_{rpqmnx}$$

Likewise the electric field components due to the x-component of magnetic current sources at $z = c$ plane are obtained as

$$E_x^{IIxc} = 0$$

$$E_y^{IIxc} = -\sum_{r=1}^{R} \sum_{p,q} B_{rpq} \sum_{m,n}^{\infty} \frac{1}{k_I} \frac{\varepsilon_{0m}\varepsilon_{0n}}{ab\sin(k_I c)} \left(k_0^2 - \left(\frac{n\pi}{b}\right)^2\right) \sin\left(\frac{m\pi x}{a}\right) \cos\left(\frac{n\pi y}{b}\right) \sin(k_I z) I_{rpqmnx}$$

$$E_z^{IIxc} = \sum_{r=1}^{R} \sum_{p,q} B_{rpq} \sum_{m,n}^{\infty} \frac{1}{k_I} \frac{\varepsilon_{0m}\varepsilon_{0n}}{ab\sin(k_I c)} \frac{n\pi}{b} \sin\left(\frac{m\pi x}{a}\right) \sin\left(\frac{n\pi y}{b}\right) \cos(k_I z) I_{rpqmnx}$$

REPORT DOCUMENTATION PAGE

Form Approved
OMB No. 0704-0188

1. AGENCY USE ONLY (Leave blank)	2. REPORT DATE	3. REPORT TYPE AND DATES COVERED
	June 2000	Contractor Report

4. TITLE AND SUBTITLE
Electromagnetic Field Penetration Studies

5. FUNDING NUMBERS
C NAS1-96013

WU 522-31-21-04

6. AUTHOR(S)
M. D. Deshpande

7. PERFORMING ORGANIZATION NAME(S) AND ADDRESS(ES)
NYMA, Inc.
NASA Langley Research Center
Hampton, VA 23681-2199

8. PERFORMING ORGANIZATION REPORT NUMBER

9. SPONSORING/MONITORING AGENCY NAME(S) AND ADDRESS(ES)
National Aeronautics and Space Administration
Langley Research Center
Hampton, VA 23681-2199

10. SPONSORING/MONITORING AGENCY REPORT NUMBER
NASA/CR-2000-210297

11. SUPPLEMENTARY NOTES
M. D. Deshpande, FDC/NYMA Inc., Hampton, VA
Langley Technical Monitor: Fred B. Beck

12a. DISTRIBUTION/AVAILABILITY STATEMENT
Unclassified-Unlimited
Subject Category 32 Distribution: Nonstandard
Availability: NASA CASI (301) 621-0390

12b. DISTRIBUTION CODE

13. ABSTRACT (Maximum 200 words)

A numerical method is presented to determine electromagnetic shielding effectiveness of rectangular enclosure with apertures on its wall used for input and output connections, control panels, visual-access windows, ventilation panels, etc. Expressing EM fields in terms of cavity Green's function inside the enclosure and the free space Green's function outside the enclosure, integral equations with aperture tangential electri fields as unknown variables are obtained by enforcing the continuity of tangential electric and magnetic fields across the apertures. Using the Method of Moments, the integral equations are solved for unknown aperture fields. From these aperture fields, the EM field inside a rectangular enclosure due to external electromagnetic sources are determined. Numerical results on electric field shielding of a rectangular cavity with a thin rectangular slot obtained using the present method are compared with the results obtained using simple transmission line technique for code validation. The present technique is applied to determine field penetration inside a Boeing-757 by approximating its passenger cabin as a rectangular cavity filled with a homogeneous medium and its passenger windows by rectangular apertures. Preliminary results for, two windows, one on each side of fuselage were considered. Numerical results for Boeing -757 at frequencies 26 MHz, 171-175 MHz, and 428-432 MHz are presented.

14. SUBJECT TERMS
EM Penetration, EM Shielding, Aperture Coupling, EM Susceptibility

15. NUMBER OF PAGES
71

16. PRICE CODE
A04

17. SECURITY CLASSIFICATION OF REPORT	18. SECURITY CLASSIFICATION OF THIS PAGE	19. SECURITY CLASSIFICATION OF ABSTRACT	20. LIMITATION OF ABSTRACT
Unclassified	Unclassified	Unclassified	UL